Politecnico di Bari

Department of Mechanics, Mathematics and Management
MECHANICAL AND MANAGEMENT ENGINEERING
Ph.D. Program
SSD: ING-IND/14–Mechanical Design and Machine Construction

Final Dissertation

STICK-SLIP TRANSITION AND DYNAMIC CYCLIC RESPONSE OF FRICTION DAMPED SYSTEMS

by
Antonio Papangelo

Referees:

Prof. A. STROZZI

Prof. N. HOFFMANN

Supervisors:

Prof. Ing. Michele CIAVARELLA

Prof. Ing. Luciano AFFERRANTE

Coordinator of Ph.D Program:

Prof. Ing. G.P. Demelio

XXIX cycle, 2014-2016

"Per aspera sic itur ad astra."

Seneca, Hercules furens, atto II v. 437

To Elena,

for having been always by my side,

since the first day of these 3 years…

Contents

Outline

This thesis is subdivided into two parts: in the first we analyze the transition from static to dynamic friction with some emphasis on the implication of using more refined friction laws (with respect to the simple Coulomb model) while in the second part we study the cyclic response of dynamical systems that experience friction. Particularly, in the first part we will take inspiration from some recent experiments from the group of Prof. Fineberg to tackle some partial slip contact problems, with the idea in mind of providing analytical models that can, in some extent, interpreter some of the numerous experimental evidences that came from the direct observation of the sliding phenomena. In the chapters 1-2 a brief introduction of the equations that govern the contact of elastic bodies and the experimental test rig used in the experiments is presented. In chapter 3 the partial slip problem of a flat square-ended punch pressed against an half-plane and tangentially loaded above the contact interface is studied, then a FEM of the Prof. Fineberg experimental test rig will be proposed to avoid the hypothesis of half-plane elasticity, with good agreement between numerical and experimental results. In chapter 4 the implications of using a slip weakening friction law instead of the classical Coulomb law are discussed and an energetic criterion for slip inception is derived, which we will call "Griffith friction model". In chapter 5, using this "Griffith friction", the partial slip problem for different plane geometries (power law punches and sinusoidal profile) is solved.

In the second part of the thesis we will focus our attention on the dynamic response of mechanical systems subjected to friction. In chapter 7 a very simple model of structure subjected to dry friction is studied, constituted by a single degree of freedom system subjected to a periodical tangential excitation and a (possibly) varying normal load. First we compare the quasi-static solution with the dynamic solution in the limit of very low excitation frequency, then we study (in the bounded regime) how the peak displacement and dissipation is related to the phase shift between the normal and the tangential load. In chapter 8 the dynamical behavior of a mass-spring-viscous damper structure linked to a massless Coulomb damper is studied with attention to the regime that minimize the vibration amplitude of the mass. Finally in chapter 9, we study a friction-excited nonlinear oscillator chain, where a polynomial nonlinearity is introduced in the system. We focus our attention on the multiplicity of solutions that are proven to exist in certain parameter ranges which leads to a bifurcation pattern similar to the snaking bifurcations. In the end conclusions and possible developments of the present work are proposed.

Part I

Part I: Stick-Slip transition in dry friction

Chapter 1

Plane contact of elastic bodies

In this chapter the essential equations for solving plane contact problems are shown. In the first section the elastic equations governing the plane elastic problem are presented, then starting form the solution for concentrated normal and tangential load, stress distribution and surface displacements for a general distribution of normal pressure and shear tractions are derived. The latter step allows to write the governing equations that solve the plane contact problem. In the last section the Cattaneo-Mindlin problem for partial slip is presented with the generalization introduced by Ciavarella and Jäger.

1.1 The elastic half-plane

Usually two elastic non-conforming bodies make contact over a region which dimension is considerably small with respect to the dimensions of the bodies. If the deformations are small, the linear small strain theory of elasticity can be used. Contact forces are confined to a small region (the area of contact) and the stresses decay rapidly from the contact region. These features allow to an approximation which is to consider each body as a semi-infinite elastic body that, in the undeformed condition, is locally flat in the region of contact. These approximations make the contact problem feasible to be solved in closed form as the shape of the bodies and the actual boundary conditions are not at play. Very few three-dimensional solution are known from elasticity, nevertheless in many situations that are of interest for engineers the displacements can be approximate to lie into a single plane $x - z$. Assume, for example, that one elastic body is very thin in the y direction with the stress σ_{yy} that is null on the two surfaces normal to the direction y: the σ_{yy} stress can be neglected and the state is called "plane stress". If, instead, the body is very long in the y direction, then the strain along y can be neglected and the body is said to be in "plane strain". For two dimensional problems a wide range of elastic solutions exist that can be used for solving contact problems (see [1], [2]).

Here we summarize the equations that govern the plane elastic problem, while a comprehensive derivation can be found in the Timoshenko and Godier book [3]. With reference to the Fig. 1.1 the equilibrium equations in the plane $x - z$ have to be satisfied

$$\begin{cases} \frac{\partial \sigma_{xx}}{\partial x} + \frac{\partial \tau_{xz}}{\partial z} = 0 \\ \frac{\partial \sigma_{zz}}{\partial z} + \frac{\partial \tau_{xz}}{\partial x} = 0 \end{cases} \tag{1.1}$$

where σ_{xx} (σ_{zz}) is the direct stress component in the x (z) direction, and τ_{xz} is the shear stress component acting on the plane of normal x in the direction z. The compatibility equation must be satisfied

$$\frac{\partial^2 \varepsilon_{xx}}{\partial z^2} + \frac{\partial^2 \varepsilon_{zz}}{\partial x^2} = \frac{\partial^2 \gamma_{xz}}{\partial x \partial z} \tag{1.2}$$

where within the small strain theory of elasticity the strain $\varepsilon_{xx}, \varepsilon_{zz}, \gamma_{xz}$ are related to the displacements in the horizontal $u(x,z)$ and vertical $v(x,z)$ direction via the relations

$$\varepsilon_{xx} = \frac{\partial u}{\partial x} \qquad \varepsilon_{zz} = \frac{\partial v}{\partial z} \qquad \gamma_{xz} = \frac{\partial u}{\partial z} + \frac{\partial v}{\partial x} \tag{1.3}$$

The compatibility equations ensure that during the deformation no holes open up and any material overlaps. If plane strain is considered $\varepsilon_{yy} = 0$ and $\sigma_{yy} = \nu(\sigma_{xx} + \sigma_{zz})$ .The last equations that must be satisfied in each point of the body are the constitutive laws. They are material dependent as describe how stresses and strains are related each other. If the body can be considered isotropic linear elastic the Hooke's law can be written

$$\begin{cases} \varepsilon_{xx} = \frac{1-\nu^2}{E}\left(\sigma_{xx} - \frac{\nu}{1-\nu}\sigma_{zz}\right) \\ \varepsilon_{xx} = \frac{1-\nu^2}{E}\left(\sigma_{zz} - \frac{\nu}{1-\nu}\sigma_{xx}\right) \\ \gamma_{xz} = \frac{\tau_{xz}}{G} = \frac{2(1+\nu)}{E}\tau_{xz} \end{cases} \tag{1.4}$$

where E is the Young modulus, G is the shear modulus and ν is the Poisson ratio of the material.

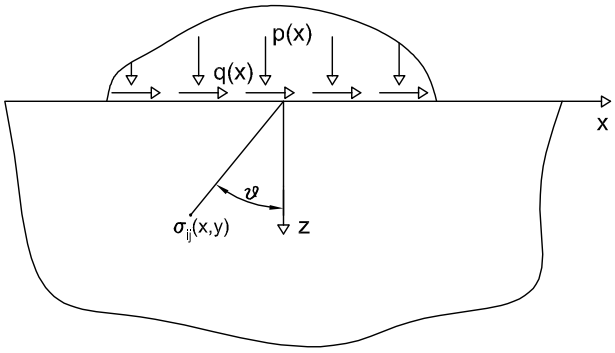

Figure 1.1 Cross-section of the elastic half-space.

To solve a plane elastic problem means to find the stress components $\sigma_{xx}, \sigma_{zz}, \tau_{xz}$ and the deformation components $\varepsilon_{xx}, \varepsilon_{zz}, \gamma_{xz}$ over the plane (x,z) using the equilibrium (1.1), compatibility (1.2) and constitutive (1.4) equations. The plane elastic problem can be reduced to a potential problem if a scalar function $\phi(x,z)$ is introduced such that the stress components can be evaluated as

$$\sigma_{xx} = \frac{\delta^2 \phi}{\delta z^2} \;\; ; \;\; \sigma_{zz} = \frac{\delta^2 \phi}{\delta x^2} \;\; ; \;\; \sigma_{xz} = -\frac{\delta^2 \phi}{\delta x \delta z} \; . \tag{1.5}$$

It can be shown that the equilibrium, compatibility and constitutive equations are automatically satisfied if the stress function ϕ satisfies the biharmonic equation

$$\frac{\delta^4 \phi}{\delta x^4} + 2\frac{\delta^4 \phi}{\delta x^2 \delta y^2} + \frac{\delta^4 \phi}{\delta y^4} = 0 \rightarrow \tag{1.6}$$

$$\nabla^4 \phi = 0 \tag{1.7}$$

The solution obtained has to satisfy the boundary conditions. In particular the half-plane surface ($z = 0$) is free of stress out of the loaded region and within the loaded region $p(x) = \sigma_{zz}(x)$ and $q(x) = \tau_{xz}(x)$, hence contact pressure will be always considered negative. Finally, far away from the loaded region, i.e. $(x, z \to \infty)$, all the stresses have to vanish. A particular contact problem can be solved when two of the four quantities $p(x), q(x), u(x,0), v(x,0)$ are specified.

1.2 Distribution of normal and tangential tractions

The analytical solution for a concentrated normal force of magnitude P per unit length was due to Flamant in 1892. One approach to solve a plane contact problem with a general distribution of normal pressure is to resort to the superposition of fundamental solutions, as that provided by Flamant. The same approach can be followed for the tangential load Q and the singular integral equations of contact can be derived which hold for a general distribution of pressure $p(x)$ and shear tractions $q(x)$.

Consider a normal load P and a tangential load Q applied on the surface of a half-plane (loads are expressed per unit length). A radial distribution of stress is obtained that is easily represented in the radial coordinate system shown in Fig. 1.1

$$\sigma_{rr}(r,\theta) = -\frac{2}{\pi r}(P\cos\theta - Q\sin\theta) \tag{1.8}$$

$$\sigma_{r\theta}(r,\theta) = \sigma_{\theta\theta}(r,\theta) = 0 \tag{1.9}$$

The corresponding Airy stress function is

$$\phi = -\frac{r\theta}{\pi}(P\sin\theta + Q\cos\theta) \tag{1.10}$$

and the stress components can be projected on the Cartesian system of reference

$$\begin{aligned}
\sigma_{xx}(x,z) &= -\frac{2}{\pi y}\left(P\sin^2\theta\cos^2\theta - Q\sin^3\theta\cos\theta\right)\\
\sigma_{zz}(x,z) &= -\frac{2}{\pi y}\left(P\cos^4\theta - Q\sin\theta\cos^3\theta\right)\\
\sigma_{xz}(x,z) &= -\frac{2}{\pi y}\left(P\sin\theta\cos^3\theta - Q\sin^2\theta\cos^2\theta\right)
\end{aligned} \tag{1.11}$$

using the transformations

$$\sin\theta = \frac{x}{\sqrt{x^2+y^2}} \tag{1.12}$$

$$\cos\theta = \frac{y}{\sqrt{x^2+y^2}} \tag{1.13}$$

Of particular importance are the surface displacements

$$u(x,0) = -P\left(\frac{\kappa-1}{8f}\right)sgn(x) + Q\left(\frac{\kappa+1}{4\pi f}\right)\ln|x| + \frac{C_1}{2f} \tag{1.14}$$

$$v(x,0) = -P\left(\frac{\kappa+1}{4\pi f}\right)\ln|x| - Q\left(\frac{\kappa-1}{8f}\right)sgn(x) + \frac{C_2}{2f} \tag{1.15}$$

where u is the tangential displacement, v is the vertical displacement, C_1, C_2 are two arbitrary constant and $sgn(x)$ function is defined as

$$sgn(x) = \begin{cases} +1, & x > 0 \\ -1, & x < 0 \end{cases} \tag{1.16}$$

Notice that due to the logarithmic term in equations (1.14) and (1.15) the displacements are unbounded and a finite value can be found only taking into account the shape of the body. A certain symmetry can be seen between the effect that the tangential force has on the tangential (normal) displacements and the normal force has on the vertical (tangential) displacements

$$-\frac{u^Q(x,0)}{Q} \propto \frac{v^P(x,0)}{P} \tag{1.17}$$

$$\frac{u^P(x,0)}{P} \propto \frac{v^Q(x,0)}{Q} \tag{1.18}$$

Equations (1.11) and (1.14)-(1.15) are the fundamental solutions sought. In fact the solution for an arbitrary distribution of pressure $p(x)$ and tractions $q(x)$ can be obtained via superposition of the solution due to concentrated loads $P = -p(\xi)\,d\xi$ and $Q = q(\xi)\,d\xi$ where $d\xi$ is an infinitesimal element on the surface in the loaded region S. Integrating over S for a given point (x, z) it is found

$$\begin{aligned}
\sigma_{xx} &= \tfrac{2}{\pi z}\left(\int_S \tfrac{p(\xi)(x-\xi)^2 d\xi z^2}{\left[(x-\xi)^2+z^2\right]^2} + \int_S \tfrac{q(\xi)(x-\xi)^3 d\xi z}{\left[(x-\xi)^2+z^2\right]^2}\right)\\
\sigma_{zz} &= \tfrac{2}{\pi z}\left(\int_S \tfrac{p(\xi) d\xi z^4}{\left[(x-\xi)^2+z^2\right]^2} + \int_S \tfrac{q(\xi)(x-\xi) d\xi z^3}{\left[(x-\xi)^2+z^2\right]^2}\right)\\
\tau_{xz} &= \tfrac{2}{\pi z}\left(\int_S \tfrac{p(\xi) d\xi z^3}{\left[(x-\xi)^2+z^2\right]^2} + \int_S \tfrac{q(\xi)(x-\xi)^2 d\xi z^2}{\left[(x-\xi)^2+z^2\right]^2}\right)
\end{aligned} \tag{1.19}$$

In the same way summing up the surface displacements due to normal and tangential forces and expressing the relations in terms of surface gradients it is found

$$\frac{\partial u}{\partial x}(x,0) = \frac{\kappa-1}{4G}p(x) + \frac{\kappa+1}{4\pi G}\int_S \frac{q(\xi)}{x-\xi}d\xi \tag{1.20}$$

$$\frac{\partial v}{\partial x}(x,0) = -\frac{\kappa-1}{4G}q(x) + \frac{\kappa+1}{4\pi G}\int_S \frac{p(\xi)}{x-\xi}d\xi \tag{1.21}$$

where κ is the Kolosov constant and in plain strain is equal to

$$\kappa = 3 - 4\nu \tag{1.22}$$

1.3 The plane contact problem formulation

1.3.1 Integral equations governing the contact problem

Consider two elastic bodies that make contact on a region S. Assume that $f_1(x), f_2(x)$ describe the profile of the upper and lower (1 & 2, respectively) contacting bodies, while T_y and R are the normal and rotational components, respectively, of the rigid body motion that brings the two bodies into contact, given in the fixed coordinate system $x - z$. The function $h(x)$ can be defined as the the amount of overlap if the bodies were allowed to interpenetrate each other freely in the undeformed state, as

$$h(x) = T_y + Rx - [f_1(x) - f_2(x)], \tag{1.23}$$

Using equation (1.21) for both bodies

$$\frac{\partial v_1}{\partial x}(x,0) = -\frac{\kappa_1-1}{4G_1}q(x) + \frac{\kappa_1+1}{4\pi G_1}\int_S \frac{p(\xi)}{x-\xi}d\xi \tag{1.24}$$

$$\frac{\partial v_2}{\partial x}(x,0) = -\frac{\kappa_2-1}{4G_2}q(x) - \frac{\kappa_2+1}{4\pi G_2}\int_S \frac{p(\xi)}{x-\xi}d\xi \tag{1.25}$$

where the change of sign in (1.25) is due to the common system of reference in which the equation are now written for both the bodies. The compatibility condition in the normal direction imposes that within the contact area S the $z-$component of relative displacements $\mathbf{v} = \mathbf{v}_1 - \mathbf{v}_2$ has to be equal to the overlap

$$v_1(x) - v_2(x) = h(x), \qquad x \in S \tag{1.26}$$

$$v_1(x) - v_2(x) > h(x), \qquad x \notin S \tag{1.27}$$

where the latter condition avoids interpenetration outside the contact area. Using equations (1.24-1.25-1.26) we write

$$\frac{1}{A}\frac{\partial h(x)}{\partial x} = \frac{1}{\pi}\int_S \frac{p(\xi)\,d\xi}{x-\xi} - \beta q(x), \qquad x \in S \tag{1.28}$$

where

$$A = \frac{\kappa_1 + 1}{4G_1} + \frac{\kappa_2 + 1}{4G_2} \tag{1.29}$$

$$\beta = \frac{G_2(\kappa_1 - 1) - G_1(\kappa_2 - 1)}{G_2(\kappa_1 + 1) + G_1(\kappa_2 + 1)} \tag{1.30}$$

the integral has to be interpreted as Cauchy Principal Value, and appropriate side conditions must be given to choose the physically meaningful solution from the space of the mathematical solutions, as discussed in the definitive treatise by Muskhelishvili [4]. These side conditions depends on the behaviour (bounded /unbounded) of the unknown functions at the ends of contact areas, and on whether the area is connected or not. Notice that A is a measure of the compliance of the bodies while β (often called, β Dundurs' parameter [5]) gives a measure of the 'elastic mismatch' between the two bodies. We will be back on this point in the next paragraph but it's worth to note that if $\beta = 0$ then the contact problem is uncoupled hence the normal problem can be solved regardless on the solution in the tangential direction.

The second integral equation defining the problem, relates to displacement of particles parallel to the surface. It reads, again using displacement derivatives, as

$$\frac{1}{A}\frac{\partial g(x)}{\partial x} = \frac{1}{\pi}\int_S \frac{q(\xi)\,d\xi}{x-\xi} + \beta p(x), \qquad x \in S \tag{1.31}$$

where $g(x)$ is the relative tangential displacements and the integral has to be interpreted again as a Cauchy Principal Value. It's worth to note that the material constants enter in the problem only through the parameters A and β thus whatever pair of materials yielding to the same parameters A, β has the same contact solution. This is useful, in particular because the contact between two elastic bodies can be reduced to the contact between an elastic and a rigid body, provided that the elastic constants of the elastic body are adjusted accordingly. This is particularly helpful in visualizing the deformation, as it can be all accommodated in one body. If the body 2 is rigid, in plane strain condition, the formulas for A, β simplifies in

$$A = \frac{1 - \nu_1}{G_1}; \qquad \beta = \frac{1 - 2\nu_1}{2(1 - \nu_1)} \tag{1.32}$$

From the equilibrium equations the resultant forces P (positive compressive force), tangential

force Q, and moment M are obtained

$$P = -\int_S p(x)\,dx \tag{1.33}$$

$$Q = +\int_S q(x)\,dx \tag{1.34}$$

$$M = -\int_S p(x)\,xdx \tag{1.35}$$

where is intended that M is the moment with respect to the origin of the coordinate system $x = 0$, and the contact area S is not necessarily connected.

1.3.2 Partial slip condition for similar materials

Consider the problem of two elastically similar bodies ($\beta = 0$) that are brought into contact by a normal load P. If the bodies are similar there will be no relative slip between the surfaces due to the application of a normal load P. Assume that at the interface Coulomb friction is postulated, that a tangential force is increased from 0 to a value $Q < fP$, where f is the unique coefficient of friction, and $g_0'(x)$ is the value of $\partial g/\partial x$ when a point of the surface first enter in the stick zone. If slip is not permitted in all the contact area then $S_{stick} \equiv S$ and $g_0'(x) = 0$ as no relative slip has occurred at the interface during the loading phase. Equation (1.31) reads

$$\frac{1}{\pi}\int_S \frac{q(\xi)\,d\xi}{x-\xi} = 0 \tag{1.36}$$

Regardless the shape of the indenter the shear traction distributions take the form

$$q(x) = \frac{q_0}{\sqrt{1-\left(\frac{x}{a}\right)^2}} \tag{1.37}$$

where a is the semi-width of the contact and $q_0 = Q/a\pi$ is easily found from the equilibrium equation. It is clear that the shear tractions are unbounded at the edge of the contact and, for non-conforming bodies, the ratio $|q(x)/p(x)| \to +\infty$ for $|x| \to a$, hence this has to be considered a limit case. More likely slip will happen at the edge of the contact and the contact zone S will be split in a slip "S_{slip}" and a stick "S_{stick}" zone. In this case not only the shear traction distribution is unknown but even the location of the slip and stick zones has to be determined. Additionally, if the Coulomb friction law is used, the shear tractions in the stick zones are limited by $f|p(x)|$

$$|q(x)| < f|p(x)|, \qquad x \in S_{stick} \tag{1.38}$$

and in the slip zones are proportional to the local pressure

$$|q(x)| = -fp(x), \qquad x \in S_{slip} \tag{1.39}$$

As friction is a dissipative phenomenon, we need to impose that the shear traction in the slip zones always oppose the relative velocity between the two bodies,

$$sgn(q(x)) = sgn\left(\frac{\partial g}{\partial t}\right), \qquad x \in S_{slip}. \tag{1.40}$$

1.3.3 The Cattaneo-Mindlin solution

The first partial slip solution was proposed in 1938 by Cattaneo [6] and later (in 1949), independently, by Mindlin [7] for the contact of elastically similar cylinders. First the normal load is applied, then the tangential load is increased from 0 to $Q < fP$. As the normal and tangential problems are uncoupled, regardless from the shear traction distribution, the pressure distribution is that found by Hertz for two-dimensional problems [1]

$$p(x) = -p_0 \sqrt{1 - \left(\frac{x}{a}\right)^2} \tag{1.41}$$

where $p_0 = \frac{2P}{\pi a}$ (see the Johnson's book for further details [2]). We have seen in the former paragraph that the surfaces are more likely to slip at the edge of the contact strip. Due to these considerations and due to the intrinsic symmetry of the problem, Cattaneo and Mindlin postulate that the stick zone will be located in the middle and will shrink as the slip zone moves forward from the edges to the middle. They assume that in the slip zone S_{slip} the Coulomb law holds, while in the stick zone S_{stick} the shear tractions distribution can be written as a correction of the full sliding term, which we denominate $q^*(x)$. Hence one has

$$q(x) = \begin{cases} -fp(x) + q^*(x), & x \in S_{stick} \\ -fp(x), & x \in S_{slip} \end{cases} \tag{1.42}$$

Defining c the semi-width of the stick area, Cattaneo and Mindlin show that $q^*(x)$ has the form

$$q^*(x) = -fp_0 \frac{c}{a} \sqrt{1 - \left(\frac{x}{c}\right)^2} \tag{1.43}$$

and the contact problem is solved. In particular the shear traction distribution is

$$q(x) = \begin{cases} -fp_0 \left[\sqrt{1 - \left(\frac{x}{a}\right)^2} + \frac{c}{a} \sqrt{1 - \left(\frac{x}{c}\right)^2} \right], & |x| \leqslant c \\ -fp_0 \sqrt{1 - \left(\frac{x}{a}\right)^2}, & c < |x| \leqslant a \end{cases} \tag{1.44}$$

and it is proven [2] that satisfies the contact conditions:

- $|q(x)| < f|p(x)|$ in the stick zone;
- rigid body displacement in the stick region;
- the shear tractions oppose the relative slip between the two contact surfaces;

Integrating $q(x)$ over the contact area the relation between the semi-width of the stick zone and the tangential load is easily found

$$\frac{c}{a} = \left(1 - \frac{Q}{fP}\right)^{1/2} \tag{1.45}$$

1.3.4 Partial slip solution for general profiles

Cattaneo-Mindlin solved the partial slip problem between two cylinders by a clever superposition of a corrective term (1.43) to the full sliding term. The form of the corrective term was found ad hoc, and not derived from general considerations, nevertheless it has to be noted that it is just

[1] Hertz found it as the limit case of a three-dimensional elliptic contact where the length of the semi-axes b is much greater than the length of the semi-axes a.

a rescaled form of the Hertzian pressure distribution (1.41). It was shown by Ciavarella ([8],[9]) and independently by Jäger [52] that for two-dimensional contact problems the corrective term is always a rescaled form of the normal problem (under the hypothesis that the contact problem is uncoupled, i.e. $\beta = 0$). This is of great importance as allows to derive the partial slip solution for many profile shapes, where the pressure distribution is usually available ([8],[9]). Note that the hypothesis $\beta = 0$ is not too restrictive, has not only elastically similar material satisfy it but even the contact of steel over rubber and, in general, all the materials that satisfy the relation

$$\frac{1-2\nu_1}{G_1} = \frac{1-2\nu_2}{G_2} \tag{1.46}$$

Here it is shown how to generally derive the form of the corrective term for a given overlap function $h(x)$. As in the standard Cattaneo-Mindlin solution we write the shear traction distribution in the stick zone as a superposition of the full sliding term and a corrective term $q^*(x)$

$$q(x) = \begin{cases} fp(x) + q^*(x), & x \in S_{stick} \\ fp(x), & x \in S_{slip} \end{cases} \tag{1.47}$$

From the integral equation for relative displacements in the tangential direction with $g_0'(x) = 0$ and $\beta = 0$ we write

$$0 = \frac{1}{\pi}\int_S \frac{q(\xi)\,d\xi}{x-\xi} = \frac{f}{\pi}\int_S \frac{p(\xi)\,d\xi}{x-\xi} + \frac{1}{\pi}\int_{S_{stick}} \frac{q^*(\xi)\,d\xi}{x-\xi} \tag{1.48}$$

where $q^*(x) = 0$ in the slip zones, by definition. From the integral equation for the normal contact (1.28) in plane strain condition

$$\frac{1}{\pi}\int_S \frac{p(\xi)\,d\xi}{x-\xi} = \frac{E^*}{2}h'(x) \tag{1.49}$$

where E^* is the composite modulus

$$\frac{1}{E^*} = \left(\frac{1-\nu_1^2}{E_1} + \frac{1-\nu_2^2}{E_2}\right) \tag{1.50}$$

Substituting (1.49) into (1.48) one obtains

$$\frac{E^* f}{2}h'(x) + \frac{1}{\pi}\int_{S_{stick}} \frac{q^*(\xi)\,d\xi}{x-\xi} = 0, \qquad x \in S_{stick} \tag{1.51}$$

$$\frac{1}{\pi}\int_{S_{stick}} \frac{-q^*(\xi)/f}{x-\xi}d\xi = \frac{E^*}{2}h'(x), \qquad x \in S_{stick} \tag{1.52}$$

that is exactly the same form as the original equation for normal contact for $\beta = 0$, with $p(x)$ replaced by $-q^*(x)/f$, and integrated only over S_{stick}. This proves the corrective term being the same form of the normal pressure, as found by Cattaneo and Mindlin. In a later paper [10] Ciavarella showed that this form of superposition is a good approximation in the general three-dimensional case. The reader is referred to ([8],[9],[10]) for further details.

Chapter 2

Fineberg's experiment

In this chapter the experimental set-up used by the Fineberg's group is described. A literature review is proposed that briefly summarize the most important results among the others. Possible interpretation of the results is presented based on the state of the art.

2.1 Introduction

We experience friction in our daily life. Essentially friction is a dissipative phenomenon due to a plethora of processes that take place at the contact interface. Despite the very complicated picture the basic concepts that govern friction have been understood thousands years ago. Trace of lubricants have been found in archeological finds dated back to about 1400 B.C. The Egyptian used lubrication for moving heavy stone statues. Figure 2.1 reports a painting found in a grotto at El-Bershed dated about 1880 B.C. which shows an officer while pouring a fluid just in front of the sledge. Note that there aren't any rollers or bearings under the sledge.

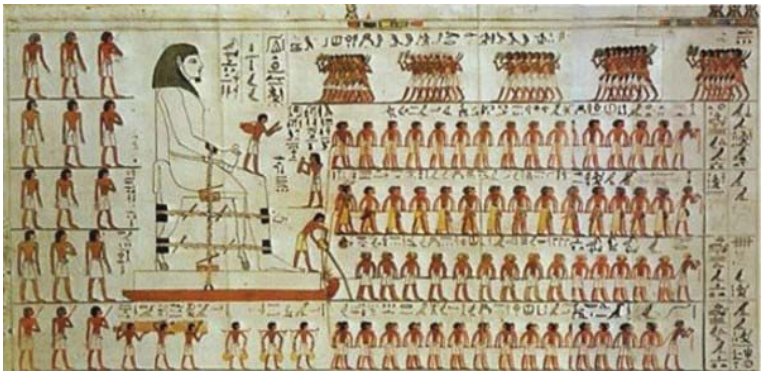

Figure 2.1 Egyptian while transporting a large stone statue on a sledge. Painting from the tomb of Tehuti-Hetep, El-Bershed (about 1880 B.C.) (adapted from [11])

The first systematic study on friction is due to Leonardo da Vinci, the eclectic Italian scientist who firstly said (I) *"Friction produces double the amount of effort if the weight be doubled"* stating the proportionality between normal and tangential load. He performed experiments with blocks of different geometries and recognized that (II) *friction is independent on the apparent area of contact.* These two laws were rediscovered and published by the french engineer Guillaume Amontons in 1699. A wide studies on friction were performed by the physicist Charles Augustin de Coulomb

in the 18th century. He showed that friction depends on the length of time that the surfaces are held in contact and (III) *is independent on the sliding velocity*, provided that it isn't too low or too high. The three laws (I)-(II)-(III) form the Amonton-Coulomb model of friction and

$$f = \frac{Q}{P} \tag{2.1}$$

is called "friction coefficient". Within this model, it is considered a constant that characterizes the couple of materials (more precisely we should write "surfaces") that make contact. The first modern work (1950) on friction is surely due to Bowden and Tabor [12]. They firstly recognize the role of roughness saying *"putting two solids together is rather like turning Switzerland upside down and standing it on Austria"* and underlined that there is a clear distinction between "apparent" and "real" contact area. In fact, the real contact area (which uniquely contribute to friction) is actually proportional to the load and this explains the first two Amonton-Coulomb model laws. Due to the fact that the contact occurs only on microscopic asperities, the pressure locally is sufficient to cause yield, hence friction is due to asperity junction plastic failure. The increasing strength of the interface instead, is possibly due to creep phenomena at asperity scale. Later on, statistical models explained that the average pressure on each asperity tends to be constant, and only the number of contacting asperities changes with increasing normal force. Greenwood and Williamson [13] confirmed the proportionality of contact area and normal force with such a statistical approach.

Yet, for many scopes (in particular for engineering applications), the Coulomb law is still very much in use, and more complicated laws are often developed empirically trying to account for the influence of other factors, such as slip distance, speed, normal load, surface conditions, temperature, etc. (see Rabinovicz, [14]). When sliding starts, thermal effects are activated, both at bulk and asperity scales, and this is usually one of the factors called upon to explain the rate-dependence of friction as part of the difference between static and dynamic friction coefficient (see Rice, [15]). Dieterich [16] and Ruina [17] (see also Dieterich [18]) suggested a rate-and-state dependent friction law to explain a large amount of laboratory data on rock friction. To summarize, while the basic law is still useful for very qualitative results, the understanding of frictional processes is still very far from even remotely completed.

2.2 Fineberg experimental set-up

Recently, an interesting series of experiments has been conducted by the group of Jay Fineberg in Israel ([19], [20], [21], [22],[23], [24], [25]), in which a rig has been built with two blocks of PMMA (polymethyl-methacrylate): the bottom layer ("base") is pushed to one side and the upper block ("sliders") is held from the top or by an optional stopper at some height from the interface. The base has dimensions ($x = 300, y = 30, z = 27$) mm while the sliders have dimensions ($x = 140, y = 6, z = 75$) mm and ($x = 200, y = 6, z = 75$) mm. The rig is very sophisticated in the measurements, since the contact area is monitored at very high rate in time ($\sim 10^5$ frames per second) and space (1280 pixel along x dimension) with laser measurements of the real contact area $A(x,t)$ which are averaged over the thickness (direction y). The contact surfaces are lapped to have a roughness of 1 μm. Additionally, a set of strain gauges is mounted on the upper block close to the interface (2 mm height) to measure near interface pressure and shear. During the experiment the slider was tangentially loaded via a "rigid" rod connected to a load cell. Generally, when overall sliding occurred, a stick slip motion initiated. Many interesting results came out from these experiments and many research group have been working on it since the last 10 years. A local ratio of τ/σ much higher than the static friction coefficient was observed [22] and dependence of macroscopic friction coefficient from the loading condition [24]. Real-time visualization of the net contact area shows a complex pattern of propagating fronts at the interface, from slow to super-shear ([22],[21]). These fronts either stop in the middle or transverse the entire interface. Notably this rich dynamics

happens before that the main slip event (overall sliding) occurs. We will concentrate our attention on the so called "precursor fronts" ([20],[21]). Figure 1 (a) of [20] shows an example of a loading curve. It is shown that before the main sliding event, during the loading phase, small drops of the tangential force Fs where observed and each drop corresponds to a slip precursor front that starts from one edge, where the load is applied, and transverse the interface ($\sim$ 80% of the Rayleigh velocity) up to a certain length l, then stops. These fronts strongly alter the contact area at the interface thus changing the interface conditions well before that the main slip event happens. Figure 1 (a) of [20] (see also [21]) shows that data taken from different experiments all collapse into a single master curve if l/L is plotted versus F_s/F_N, with L the x dimension of the slider and F_N the normal force applied. It has been shown that this linear behavior diverges when the precursors length reaches about $L/2$.

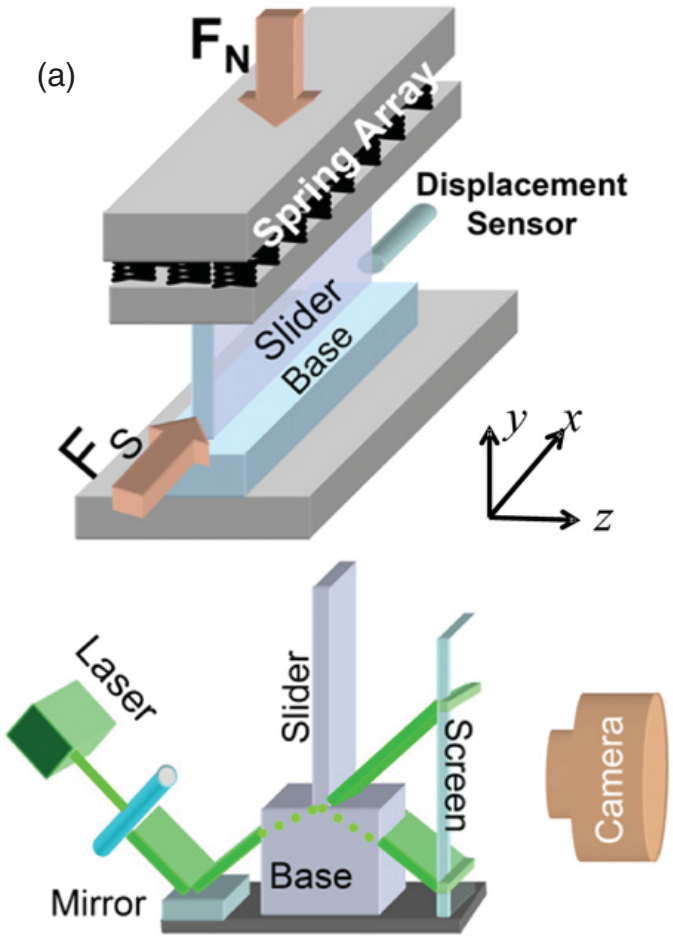

Figure 2.2 Fineberg's experimental setup (adapted from [21])

A great effort has been made to reproduce the complex dynamic at the interface using 1D models ([26],[27],[28],[29]), 2D spring-block models ([30],[31]), 2D finite element models ([32],[33]). In particular in [33] a model based on Linear Elastic Fracture Mechanics (LEFM) has been proposed, which can quantitatively predict precursor length. On the other hand little effort has been made so far (except perhaps [34], [35]) of quasi-static analysis for the problem, despite clearly the loading

regime is well within quasi-static limits. One concern is that there are many effects at play which don't permit a simple analysis, besides the dynamic propagation of slip fronts: the nature of the contact is not easily manageable with half-space elasticity, since there are end effects at the corners of the elastic flat block which depend on Poisson's frustration, and this has been also remarked in some of the most recent papers where the strong effect of tilting of a small angle has also been noticed, which affects the apparent friction coefficient for the onset of motion [24].

In the part I of this thesis a quasi-static analysis of Fineberg experiments will be proposed ([36],[37],[38]).

Chapter 3

A Cattaneo-Mindlin problem for a rigid punch with tangential load applied above the interface line

In this chapter analytical and numerical models, inspired to the Fineberg experimental set-up, are proposed to study the partial slip contact problem of a rigid punch with tangential load applied above the interface line using a quasi-static approach. In particular it will be shown that half-plane elasticity is not able to reproduce the experimental results found by Fineberg, while a FEM does.

3.1 Analytical solution

3.1.1 Problem statement

An idealized model is considered constituted by a rigid punch with tangential load applied above the interface line that is in contact with an elastic incompressible half-plane. Friction is described using the Coulomb law, with no difference between static and dynamic friction coefficient. With these hypothesis a closed form analytical solution is derived for the slip front quasi-static propagation.

In order to use half-plane elasticity to solve the partial slip problem in Finegerg's setup the top block is assumed to be rigid so that detailed elasticity of the square-cornered punch is avoided, and it indents an incompressible half-space, so that there will be no elastic coupling. The loading will be that of a centered normal load (P) and a tangential load (Q) applied in sequence, but the tangential load will be applied at a given height so as to reproduce the stopper in the Fineberg rig, and induce tilting effect which is not well known in the standard Cattaneo-Mindlin problem for the Hertzian (quadratic gap) problem ([2], [39]). The normal load (P) will remain applied at $x = 0$ without being affected by the tilt of the upper block (see Fig. 3.1).

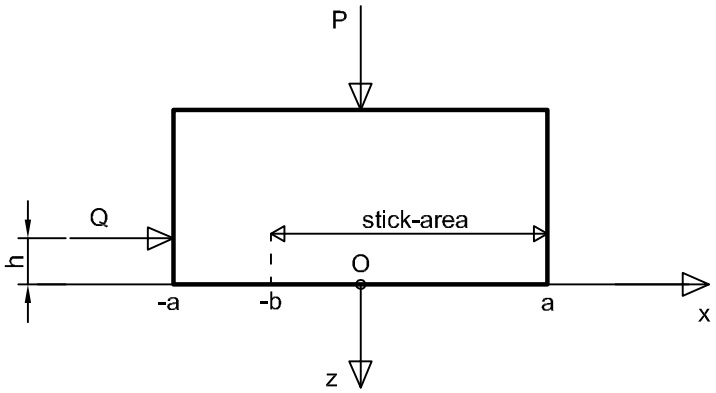

Figure 3.1. Geometrical model considered.

From classical half-planes elasticity, ([2], [39]), the general relations between the traction distributions (pressures p and shear q) and the derivative of surface displacements of an elastic incompressible half space (plane strain condition) indented by a rigid punch are the following Cauchy integral equations

$$\frac{E^*}{2}\frac{dh_p(x)}{dx} = \frac{1}{\pi}\int_{-a}^{a}\frac{p\left(\xi\right)d\xi}{x-\xi} \tag{3.1a}$$

and

$$-\frac{E^*}{2}\frac{du_1(x)}{dx} = \frac{1}{\pi}\int_{-a}^{a}\frac{q\left(\xi\right)d\xi}{x-\xi} \tag{3.1b}$$

In general, E^* is the elastic composite modulus, $\frac{1}{E^*} = \frac{1-\nu_1^2}{E_1} + \frac{1-\nu_2^2}{E_2}$ but being $\nu_1 = 0.5$ (incompressible) ex hypothesis, and $E_2 = \infty$ (rigid flat punch), $\frac{1}{E^*} = \frac{3}{4E_1}$ so that Dundurs' second parameter is zero and the problem of normal and tangential contacts are uncoupled ([2], [39]). Further, u_1 are tangential displacements in the halfplane, and $h_p = h_{1p} - h_{2p}$ is the total gap between the two profiles, but in this case both profiles are flat so the gap depends uniquely on tilt and vertical approach.

The tangential load Q is applied above the line of contact causing a moment $M = Qh$, thus the punch is tilted of an angle θ_t. The contact pressures can be expressed as [40]:

$$p\left(x\right) = \frac{P}{\pi\sqrt{a^2-x^2}}\left(1 + \frac{2Qh}{P}\frac{x}{a^2}\right) \tag{3.2}$$

Since it is customary to work with displacement derivatives in halfplane elasticity, we use the equations (3.1a) and (3.2) to find the tilt angle θ_t:

$$\theta_t = -\frac{dh_p(x)}{dx} = -\frac{2}{\pi E^*}\int_{-a}^{a}\frac{p\left(\xi\right)d\xi}{x-\xi} = \frac{4Qh}{E^*\pi a^2} \tag{3.3}$$

i.e. $h'_{2p}(x) = \frac{4Qh}{E^*\pi a^2}$.

To ensure complete contact, $p(x)$ must be greater than zero on the whole contact surface, and in particular on the left corner

$$p(-a) \geqslant 0 \Rightarrow Q \leq \frac{fPa}{2fh} = fP\alpha = Q_t \tag{3.4}$$

where Q_t is the tangential force at which lift-off occurs, and we have introduced an important parameter for our investigation

$$\alpha = \frac{a}{2fh} > 0. \tag{3.5}$$

The contact starts always from a full-stick condition. In these early stages, the tangential pressures distribution is:

$$q(x) = \frac{Q}{\pi\sqrt{a^2 - x^2}} \tag{3.6}$$

The standard Cattaneo-Mindlin partial slip solution can be obtained based on the Coulomb-friction model for which the slip starts when:

$$\frac{q(x)}{p(x)} \geqslant f \tag{3.7}$$

which in our case occurs at $x = -a$ (the first point where the condition in eq. (3.7) is verified):

$$\frac{q(-a)}{p(-a)} \geqslant f \Rightarrow Q \geqslant \frac{fP\alpha}{1+\alpha} = Q_{os} \tag{3.8}$$

Notice that comparison of eq. (3.4) and eq. (3.8) gives:

$$Q_t = fP\alpha > \frac{fP\alpha}{1+\alpha} = Q_{os} \tag{3.9}$$

This means that slip between the two surfaces starts always before the contact becomes incomplete.

Complete contact up to full sliding occurs if

$$fP = Q_{fs} < Q_t = fP\alpha \Rightarrow \alpha > 1 \tag{3.10}$$

Otherwise ($\alpha < 1$), the punch will tilt at $Q = Q_t$ and the normal pressure will vanish at $x = -b$ while it will remain singular at $x = a$. It is convenient to define a new system of reference $\widehat{x'O'z'}$ that has the propriety to remain centered with respect to the stick area. In this reference system the pressures distribution will be (we shall return later with more details):

$$p(x') = \begin{cases} 0 & -a < x < -b \\ \frac{P}{\pi a'}\sqrt{\frac{a'+x'}{a'-x'}} & -b < x < a \end{cases} \tag{3.11}$$

where:

$$a' = a\left(2 - \frac{Q}{\alpha P f}\right); x' = x - (a - a') \tag{3.12}$$

The tip over condition $a' = 0$ is reached when:

$$2a = \frac{2Qh}{P} \Rightarrow Q_{to} = 2fP\alpha \tag{3.13}$$

thus full sliding will occur before tip over if:

$$2fP\alpha = Q_{to} > Q_{fs} = fP \tag{3.14}$$

i.e. for $\alpha > 1/2$. In the next sections, the cases for $\alpha > 1$ (complete contact), $1/2 < \alpha < 1$ (partial contact) and finally $\alpha < 1/2$ will be treated separately. Figure 3.2 summarizes the three possible scenarios based on the value of the parameter α. For each row the tangential load is increased from the left to the right and each sketch represents the qualitative stick/slip condition for a certain value of Q.

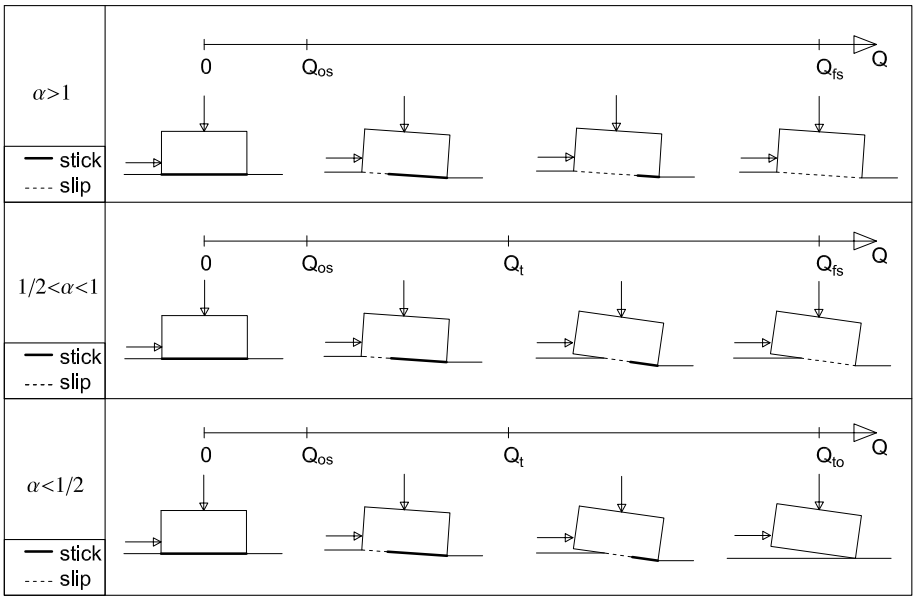

Figure 3.2. Possible scenario as a function of α. The stick zone is represented with a bold solid line, while the slip state is drawn with a dashed line.

3.1.2 Complete contact ($\alpha > 1$)

As stated above, when $\alpha > 1$ the transition from partial slip to the fully sliding condition is always with a complete contact between the two surfaces. The point of first slip is at $x = -a$ for $Q = Q_{os}$ (eq. (3.8)). When $Q_{os} < Q < Q_{fs}$ a partial slip condition must be defined. The Cattaneo-Mindlin generalized solution (see [6],[8],[10]) considers the tractions distribution on the contact area as the superposition of the full-sliding solution $q(x) = fp(x)$ for $-a < x < a$ and a corrective distribution $q^*(x)$ for $-b < x < a$ such that:

$$q(x) = \begin{cases} fp(x) & -a < x < a \\ fp(x) + q^*(x) & -b < x < a \end{cases} \tag{3.15}$$

and equilibrium requires

$$\int_{-a}^{a} q(x)dx = \int_{-a}^{a} fp(x)dx + \int_{-b}^{a} q^*(x)dx = Q \tag{3.16}$$

This results in the following integral equation

$$\frac{2(1-\nu_1^2)}{\pi E_1} \int_{-a}^{a} \frac{q(\xi)d\xi}{x-\xi} = -\frac{du_x(x)}{dx} = 0 \quad -b < x < a \tag{3.17}$$

with

$$q^*(-b) = 0 \tag{3.18}$$

where eq. (3.17) represents the stick condition and eq.(3.18) means that the corrective term must be zero at the stick-slip boundary[1]. Condition (eq.(3.17)), with (3.3), gives

$$\int_{-b}^{a} \frac{q^*(\xi)\, d\xi}{x-\xi} = \frac{1}{\alpha} \frac{Q}{a} \tag{3.19}$$

[1] In chapter 5 we will introduce a Griffith criterion for friction which leads to singular shear tractions in $x = -b$. See Appendix A to check how the shear traction distribution can be obtained when a Griffith friction model is introduced.

This is a singular integral equation of the first kind and its general solution is:

$$q^*(x) = -\frac{2fQh/a^2}{\pi^2\sqrt{(x+b)(a-x)}}\int_{-b}^{a}\frac{\sqrt{(s+b)(a-s)}}{x-s}ds + \frac{C}{\pi^2\sqrt{(x+b)(a-x)}} \tag{3.20}$$

where

$$C = \pi\int_{-b}^{a} q^*(x)\,dx = \pi(Q - fP) \tag{3.21}$$

By replacing $s = s' + \frac{a-b}{2}$, integral in eq. (3.20) can be solved giving

$$q^*(x) = \frac{-2fQh/a^2(x + \frac{b-a}{2}) + (Q - fP)}{\pi\sqrt{(x+b)(a-x)}} \tag{3.22}$$

and to fulfill the condition (eq.(3.18)), we have

$$1 + \frac{b}{a} = 2\alpha\left(\frac{fP}{Q} - 1\right) \tag{3.23}$$

The length of the slip zone is therefore:

$$\frac{l}{a} = 1 - \frac{b}{a} = 2\left[1 - \alpha\left(\frac{fP}{Q} - 1\right)\right] \tag{3.24}$$

and this dimensionless ratio is plotted in Fig. 3.3 as a function of tangential dimensionless load, for $\alpha = 1, 2, 4$. Clearly, the transition is most abrupt the higher is α and otherwise it includes a transition region. For example, for $\alpha = 1$, slip doesn't start until $\frac{Q}{fP} = 0.5$ and only after this limit, the transition starts. For higher α, the minimum $\frac{Q}{fP}$ is even higher. Notice that this paragraph includes $\alpha > 1$ case only, and hence for $\frac{Q}{fP} < 0.5$, there is no slip in this regime.

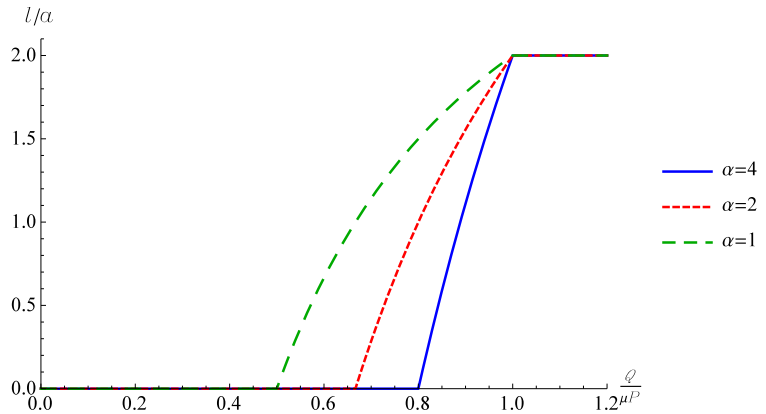

Figure 3.3. Dimensionless slip distance l/a as a function of $\frac{Q}{fP}$ for different values of $\alpha = [1 - 2 - 4]$.

Deriving b/a by eq.(3.23) and replacing it in eq.(3.22), $q^*(x)$ can be expressed as:

$$q^*(x) = -\frac{Q/\alpha}{\pi a}\sqrt{\frac{x+b}{a-x}} \quad -b < x < a \tag{3.25}$$

Thus the general form of $q(x)$ is:

$$q(x) = \begin{cases} fp(x) & -a < x < a \\ fp(x) - \frac{Q/\alpha}{\pi a}\sqrt{\frac{x+b}{a-x}} & -b < x < a \end{cases} \tag{3.26}$$

Here we plot the traction $q(x)$ and the pressure $p(x)$ for $\alpha = 2$ and $\frac{Q}{fP} = 0.75$ made dimensionless with the mean pressure $\overline{p}$. Notice how slip occurs from the left corner inwards.

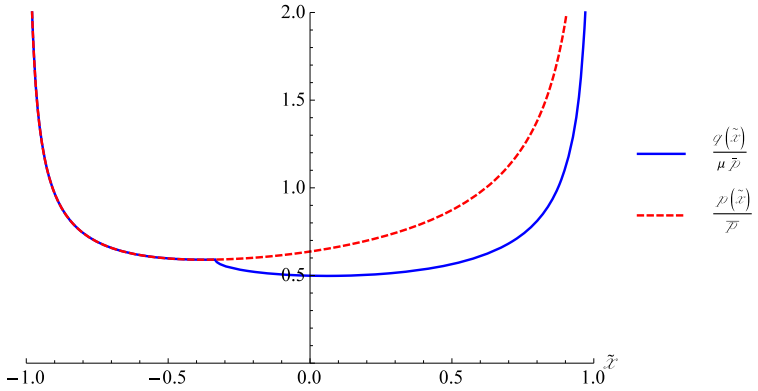

Figure 3.4. Dimensionless shear traction $\frac{q(\widetilde{x})}{f\overline{p}}$ and pressure $\frac{p(\widetilde{x})}{\overline{p}}$ for $\alpha = 2$ and $\frac{Q}{fP} = 0.75$, with $\widetilde{x} = x/a$.

3.1.3 Slip in full contact followed by slip in partial contact $(1/2 < \alpha < 1)$

As in the previous case, the contact starts from complete contact in full stick condition. When $Q > \frac{fP\alpha}{1+\alpha}$, the two surfaces start to slip, keeping a complete contact condition till $Q < fP\alpha$, at which point a partial slip condition with incomplete contact takes place, as the normal pressure at the left edge of the punch becomes zero (eq. (3.4)) and the punch starts to separate from the half-space. Hence, for $fP\alpha < Q < fP$ there will be a partial contact status and the tractions distribution will be given by a partial slip condition. The contact area decreases from $2a$ to $2a'$. The normal load P is no longer centered with respect to the new contact area of width $2a'$ and the equivalent moment applied to the punch is therefore $Qh - P(a - a')$. The pressures distribution in the coordinates $x' = x - (a - a')$ is:

$$p\,(x') = \frac{P}{\pi\sqrt{a'^2 - x'^2}}\left(1 + \frac{2[Qh - P(a - a')]}{P}\frac{x'}{a'^2}\right) \tag{3.27}$$

Eq. (3.27) differs from eq. (3.2) only for the term $P(a - a')$ in the computation of the global moment with respect to the new center. By putting $p(x' = -a') = 0$ the expression for a' is obtained:

$$a' = a\left(2 - \frac{Q}{\alpha P f}\right) \tag{3.28}$$

The normal pressures distribution is reported in eq. (3.11). The procedure for the computation of b' is the same as for the complete contact; the only difference is that this time the Cauchy integral of the full sliding component of the shear traction leads to:

$$\frac{f[Qh - P(a - a')]}{a'^2}(a' + b') + (Q - fP) = 0 \Rightarrow 1 + \frac{b'}{a'} = 2\left(1 - \frac{Q}{fP}\right) \tag{3.29}$$

and hence the results plotted in Fig. 3.5.

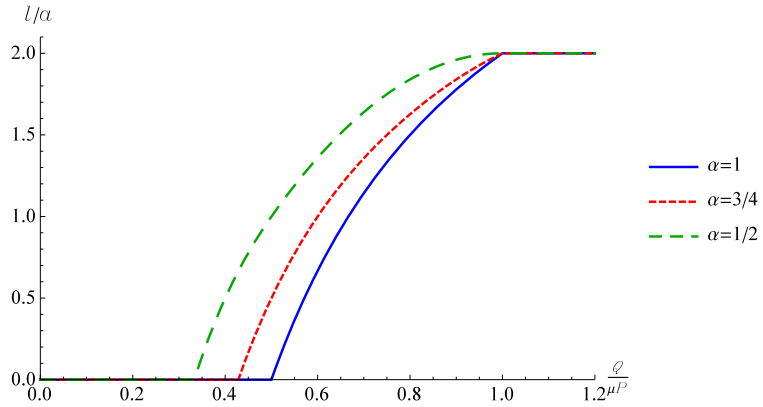

Figure 3.5. Dimensionless slip distance l/a as a function of $\frac{Q}{fP}$ for different values of $\alpha = [1 - 3/4 - 1/2]$.

In the slip region $(-a' < x' < -b')$, the tractions distribution is therefore:

$$q(x') = fp(x') = \frac{fP}{\pi a'}\sqrt{\frac{a'+x'}{a'-x'}} \tag{3.30}$$

In the stick region $(-b' < x' < a')$ the tractions distribution is given by the superposition of $fp(x')$ and $q^*(x')$. To find the corrective term $q^*(x')$

$$\int_{-b'}^{a'} \frac{q^*(\xi)\,d\xi}{x'-\xi} = -\int_{-a'}^{a'} \frac{fp(\xi)\,d\xi}{x'-\xi} = \frac{2f[Qh - P(a-a')]}{a'^2} \tag{3.31}$$

If we replace in (3.25) $\frac{1}{\alpha}\frac{Q}{a}$ with $\frac{2f[Qh-P(a-a')]}{a'^2}$ of (3.31) we obtain the new corrective term $q^*(x')$:

$$q^*(x') = -\frac{2f[Qh - P(a-a')]}{\pi a'^2}\sqrt{\frac{b'+x'}{a'-x'}} \tag{3.32}$$

In the stick region $(-b' < x' < a')$ the tractions distribution hence simplifies to:

$$q(x') = \frac{fP}{\pi a'}\left(\sqrt{\frac{a'+x'}{a'-x'}} - \sqrt{\frac{b'+x'}{a'-x'}}\right) \tag{3.33}$$

which together with the pressure is plotted, in dimensionless form, in Fig. 3.6, 3.7 for $Q/fP = 0.5, 0.8$, respectively.

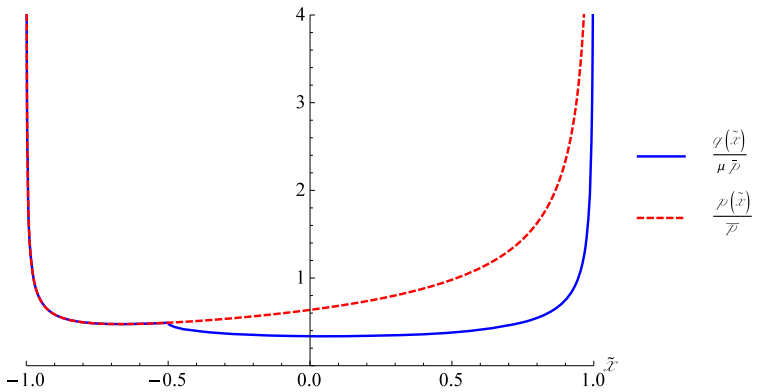

Figure 3.6. Dimensionless shear traction $\frac{q(\widetilde{x})}{f\overline{p}}$ and pressure $\frac{p(\widetilde{x})}{\overline{p}}$ for $\alpha = 0.75$ and $\frac{Q}{fP} = 0.5$ (complete contact + partial slip status), where $\widetilde{x} = x/a$.

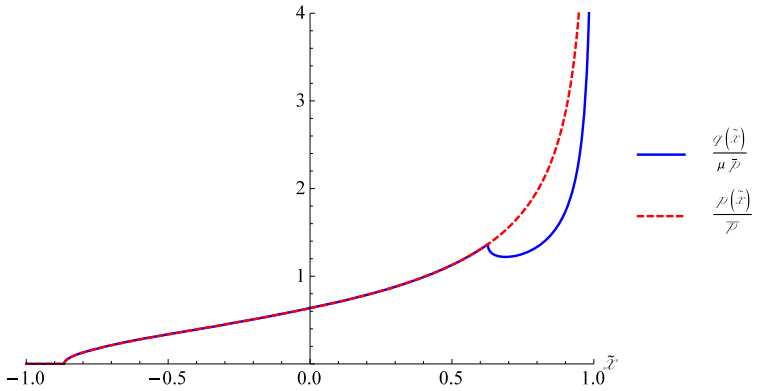

Figure 3.7. Dimensionless shear traction $\frac{q(\widetilde{x})}{f\overline{p}}$ and pressure $\frac{p(\widetilde{x})}{\overline{p}}$ for $\alpha = 0.75$ and $\frac{Q}{fP} = 0.8$ (partial contact + partial slip status), where $\widetilde{x} = x/a$.

3.1.4 Slip in full contact, slip in incomplete contact, tip over ($\alpha < 1/2$)

If $\alpha < 1/2$, then upon increasing the tangential force, we have full stick up to $Q = \frac{fP\alpha}{1+\alpha}$. Then, the contact status evolve as for the case $1/2 < \alpha < 1$ except that when the load reaches $Q = 2fP\alpha$ the punch tips over. (Thus we lose contact before that the full sliding load $Q = fP$ is reached). An example of how the slip proceeds into the interface is shown in Fig. 3.8 while Fig. 3.9 reports the dimensionless shear tractions and pressure distribution for $\alpha = 0.25$ and $\frac{Q}{fP} = 0.3$.

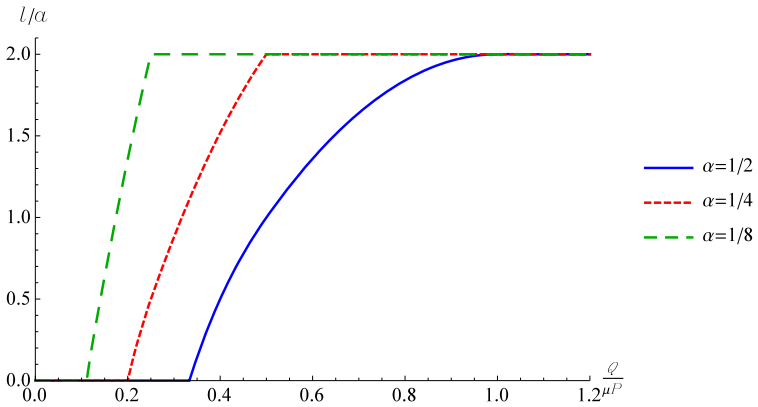

Figure 3.8. Dimensionless slip distance l/a as a function of $\frac{Q}{fP}$ for different values of $\alpha = [1/2 - 1/4 - 1/8]$.

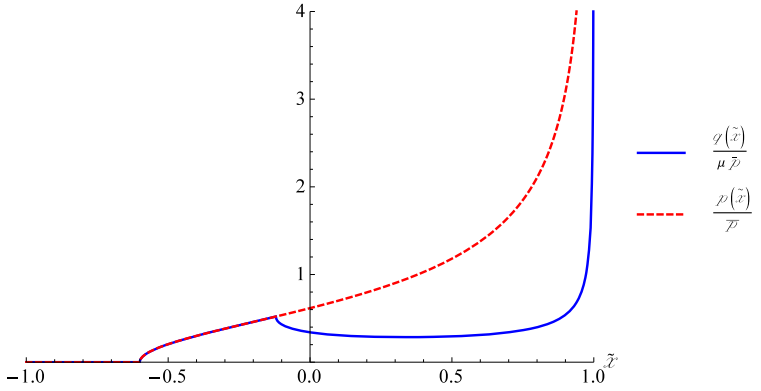

Figure 3.9. Dimensionless shear traction $\frac{q(\widetilde{x})}{f\overline{p}}$ and pressure $\frac{p(\widetilde{x})}{\overline{p}}$ for $\alpha = 0.25$ and $\frac{Q}{fP} = 0.3$ (partial contact + partial slip status), where $\widetilde{x} = x/a$.

Figure 3.10 collects all the three cases to have a better comparison of the three regimes: $\alpha < 1/2$, $1/2 < \alpha < 1$,$\alpha > 1$.

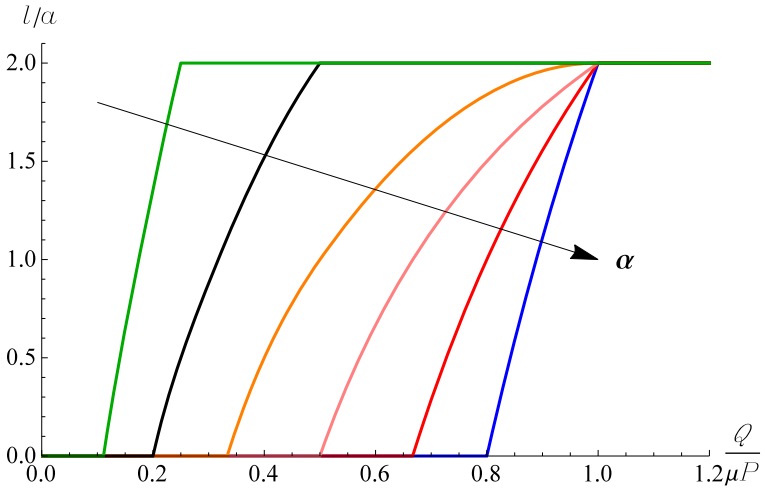

Figure 3.10. Dimensionless slip distance l/a as a function of $\frac{Q}{fP}$ for different values of $\alpha = [4 - 2 - 1 - 1/2 - 1/4 - 1/8]$.

3.2 FEM modelling

3.2.1 The Finite Element Model

In the previous section halfplane elasticity has been used to study the precursor length in an idealized version of Fineberg's setup. We have seen that the dimensionless length of the precursor fronts l/L depend on the ratio F_S/F_N and on a parameter α that is inversely proportional to the height of application of the tangential force. The curves don't collapse on a single master curve in this analytical model as found in Fineberg's experiments. Here a FEM analysis is proposed, taking into account geometry and elasticity, of the actual experimental test rig. The finite element model of the two blocks has been built using ANSYS. The geometry is presented in Fig. 3.11: the upper block unit length $L_1 * H_1 * Z_1$ and the bottom block $L_2 * H_2 * Z_2$. Different samples were used

during the experiments thus we will clarify the dimensions of the two blocks through the text. The bottom block is constrained to have the nodes at the bottom and right line fixed (Fig. 3.11).

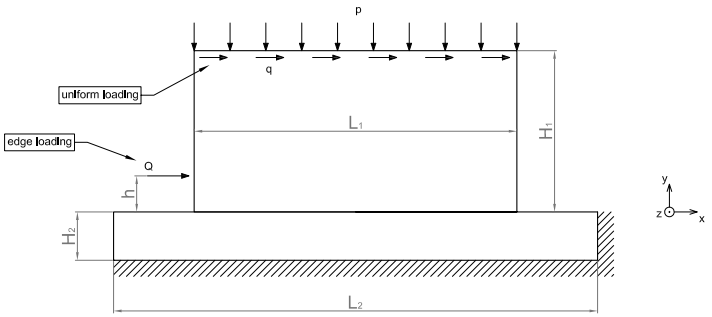

Figure 3.11. Geometrical scheme with applied constraints and loads. (a) edge loading configuration (length in [mm])

A plain strain condition is applied to the bottom block while a plain stress state is applied to the upper block. The quadratic element PLANE 183, with 8 nodes, is used to mesh the two blocks. At the interface the plane elements have been coupled with the elements CONTACT172 and TARGET169. The mesh grid was created to be parametric and structured, driving the code during the mesh operations using mesh controls, and defining proper areas and lines. The contact is defined to be surface-to-surface between two flexible bodies. The option "Surface Projection Based Contact" is used which allows to manage even large slip and nonconforming discretization across the boundary. For the solution of the contact problem the Augmented Lagrangian algorithm is adopted which demonstrated to be stable enough to manage our problem in reasonable time (1 simulation takes nearly 5 minutes using a standard PC desktop). As a drawback this kind of algorithm allows some spurious displacements even in the stick area. We overcame this limit setting manually an admissible slip in the stick area 1 orders of magnitude lower than the default value. Friction has been introduced using the Coulomb model with only one friction coefficient. First the normal load was applied evenly distributed on the top of the upper block, later the tangential load was applied on the left edge in displacement control (Fig. 3.11). The Young modulus is $E = 3100$ MPa while the Poisson ratio is $\nu = 0.35$.

3.2.2 Calibration of the model

To validate our FEM the analytical solution presented in the previous section is used, which is valid for a rigid punch pressed against an elastic halfplane with Poisson ratio $\nu = 0.5$ in a way that elastic coupling is avoided. In Fig.3.12 we report the solid lines which refer to the analytical solution (3.24) and the dots which refer to the FEM results obtained using $P = 1200$ N, $f = 0.5$, and the in plane dimensions of the blocks respectively $(L_1 * H_1) = (200 * 100)$ [mm] and $(L_2 * H_2) = (300 * 30)$ [mm]. The agreement is satisfactory.

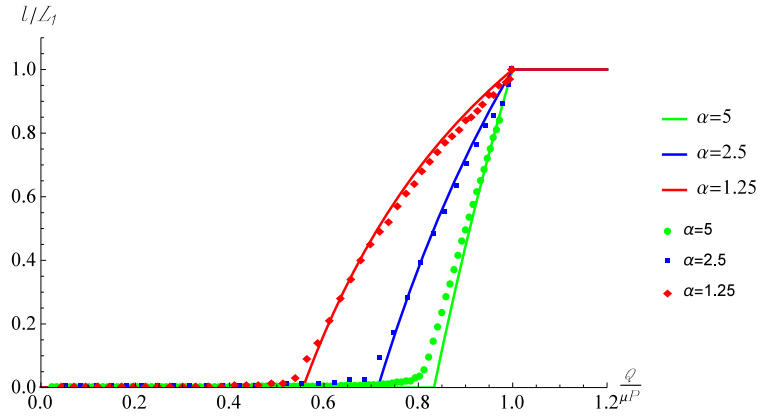

Figure 3.12. Length of the slip front made dimensionless using the width of the punch L_1 for 3 values of the dimensionless parameter $\alpha = [1.25 - 2.5 - 5]$

3.2.3 Edge Loading: Influence of the height h

The influence that the height of application of the tangential load has on the precursor propagation is investigated here. We apply a normal load $P = 3000$ N and we chose $f = 0.47$, then compared the results obtained with the experiments ([20],[21]). The dimensions of the blocks (in [mm]) are $(L_1 * H_1 * Z_1) = (140 * 80 * 6)$ and $(L_2 * H_2 * Z_2) = (300 * 30 * 30)$. The results are summarized in Figure 3.13 and show a semi-quantitative agreement with the experiments. In particular we find that the height h influences the value of Q/P at which the precursor front starts developing as observed in the experiments; as soon as the fronts start they merge into one single master curve. These aspects qualitatively agree with what the experiments showed, and with numerical results published by Tromborg *et al.* [30], (b) Taloni *et al.* [35], (c) Kammer *et al.* [33].

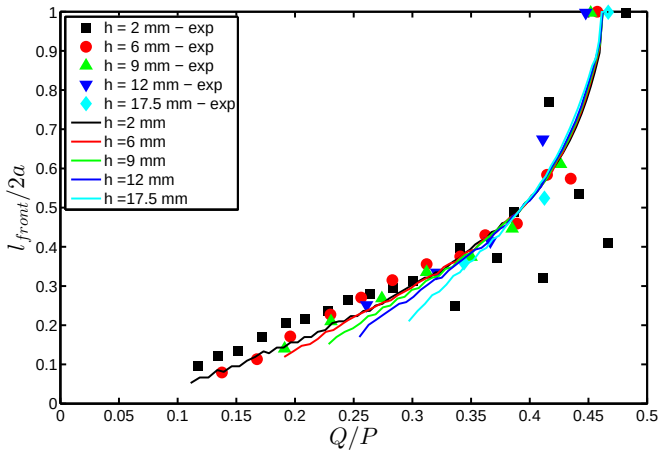

Figure 3.13. Length of the precursor fronts: discrete values from experiments, solid lines from FEM.

In Fig. 3.14 we plot the front length vs Q/P for 2 sizes of the slider ($L = 140$ and 200 mm) and different normal forces ($F_N = 2.7, 3.3, 2.6, 3.5$ kN) compared with the experimental results in

[20] (their Fig. 2 (c)). The numerical results (solid lines) and the experimental results (dots) are in good agreement.

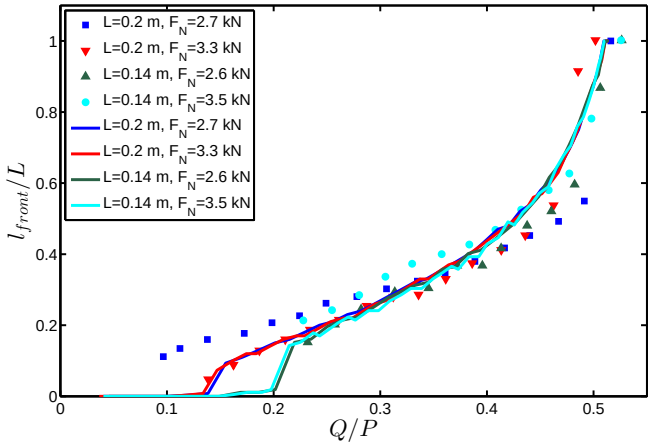

Figure 3.14. length of the front vs Q/P for 2 sizes of the slider ($L = 140$ and 200 mm) and different normal forces ($F_N = 2.7, 3.3, 2.6, 3.5$ kN)

3.3 Conclusions

Inspired by Fineberg's experiments the Cattaneo-Mindlin problem for a square-ended block has been studied. First an idealized model has been studied constituted by a rigid flat punch in contact with an halfplane. The tangential load is applied at a certain height with respect to the interface. We have found a parameter $\alpha = \frac{a}{2fh}$ which governs the possible regimes: Complete contact ($\alpha > 1$); Slip in full contact followed by slip in partial contact ($1/2 < \alpha < 1$); Slip in full contact, slip in incomplete contact, tip over ($\alpha < 1/2$). For each regime the full solution of traction distributions and the length of the slip zone has been provided. As the latter depend on the height of application of the tangential load and hence on α doesn't permit a collapse of the curves, contrary to the data shown by Fineberg. The deviations from halfplane elasticity (finite thickness of the bottom block, Poisson's ratio effects due to finiteness of the top square-ended block) don't allow to obtain a closed form solution. To overcome these limits we have developed a 2D FEM of the Fineberg's test rig. Results obtained numerically are in quantitative agreement with the experimental results, and prove that the collapse obtained in Fineberg's experiment can be obtained only if the actual geometry and length scales of the test rig are considered.

Chapter 4

Implications of slip-weakening friction laws

In this chapter we will focus our attention on the implications of using a more refined friction law (slip weakening) in contact problems. We will show that if the transition from the static to the dynamic friction coefficient is fast enough the shear traction distribution can be effectively approximated by the Linear Elastic Fracture Mechanics (LEFM) theory which, in the limit, imply an infinite local static friction coefficient at the asperity scale and lead to a Griffith friction model. These findings are corroborated by measurements of ratio τ/σ as high as 5 in Fineberg's experiments [22] and in the effectiveness of using LEFM for predicting precursor length [33]. In the second part of the chapter partial slip solutions for some profiles are presented (within the halfplane elasticity framework) using a Griffith friction model.

4.1 Introduction

If a deformable structure with frictional interfaces is subjected to loads that are insufficient to cause gross slip (sliding), the deformation of the components generally permits some local regions of 'microslip' at the nominally stuck contact interfaces. When the loading is periodic, these regions contribute to the energy dissipation in the structure and hence influence the dynamic behaviour ([41], [42]). Also, cyclic microslip can eventually lead to the initiation and propagation of fretting fatigue cracks [43].

Most of the extensive literature on problems involving microslip assumes that Coulomb's friction law applies — i.e.

$$\mathbf{q} = -fp\,\frac{\dot{\mathbf{u}}}{|\dot{\mathbf{u}}|}\,; \quad \dot{\mathbf{u}} \neq 0 \tag{4.1}$$

$$|\mathbf{q}| \leq fp\,; \qquad \dot{\mathbf{u}} = 0\,, \tag{4.2}$$

where $\mathbf{q}$ is the frictional (tangential) traction, p is the contact pressure, $\dot{\mathbf{u}}$ is the local microslip velocity, and f is the coefficient of friction. In particular, it is usually assumed that the same coefficient f governs both the slip and stick regions.

By contrast, dynamicists and tribologists often make a distinction between static and dynamic friction [14], so that equations (4.1,4.2) are replaced by

$$\mathbf{q} = -f_d\,p\,\frac{\dot{\mathbf{u}}}{|\dot{\mathbf{u}}|}\,; \quad \dot{\mathbf{u}} \neq 0 \tag{4.3}$$

$$|\mathbf{q}| \leq f_s\,p\,; \qquad \dot{\mathbf{u}} = 0\,, \tag{4.4}$$

where f_s, f_d are the static and dynamic friction coefficients respectively. In particular, if $f_s > f_d$, this friction law provides a mechanism for 'stick-slip' frictional vibrations [44]. Numerous experimental investigations have shown differences between static and sliding friction (e.g. [45]). These differences are generally small for dry metals [46], but can be substantial for earthquake fault mechanics, where ratios as high as ten between the coefficients have been reported [47]. Rice in 1996 [48] characterizes such interfaces as 'strong but brittle'.

A higher coefficient of static friction can to some extent be explained by noting that the formation of adhesive bonds, which forms the basis of Bowden and Tabor's friction theory [12], will be enhanced by diffusion if asperities remain in contact for some period of time. Similar arguments can be used to justify the 'rate-state' friction model ([17], [49]).

In this section we shall examine the effect of introducing a higher coefficient of static friction on problems involving microslip. In the interests of simplicity, we shall restrict attention to cases where Dundurs' parameter $\beta = 0$ ([2]), so there is no coupling between normal and tangential loading, and the contact pressure can be determined without reference to the friction law. Also, we shall illustrate our ideas in the context of the two-dimensional Hertz problem, since this is susceptible to simple analytical solutions, but extension to other two-dimensional cases, and to the axisymmetric Hertz problem is routine.

4.2 Evolution of frictional traction distributions

4.2.1 Classical solutions

Cattaneo [6] and later Mindlin [7] considered the case where two elastic bodies are first pressed together by a normal force P, which is then held constant whilst a monotonically increasing unidirectional force Q_x is applied. The profile of the bodies was characterized by a quadratic initial gap function $h_0(x, y) = Ax^2 + By^2$, so that the normal loading phase is defined by the classical Hertz theory. Cattaneo and Mindlin then showed that, subject to a small approximation associated with the local slip direction [50], the shear traction distribution has the form

$$q_x(x, y) = f\,[p(x, y) - p^*(x, y)]\ , \tag{4.5}$$

where $p(x, y) > 0$ is the contact pressure and $p^*(x, y)$ is the contact pressure that would be developed at some smaller normal force P^* given by

$$P^* = P - \frac{Q_x}{f}\ . \tag{4.6}$$

Ciavarella [8] and Jäger [52] have since shown that this form of superposition is exact for any initial gap function $h_0(x)$ in the two dimensional case, and that it is a good approximation in the general three-dimensional case [10].

4.2.2 Static and dynamic friction

Now consider the case where $f_s > f_d$ and the loading scenario is the same as in the Cattaneo-Mindlin problem. We assume the existence of a slip zone in which $q_x(x, y) = f_d\, p(x, y)$, so we write the complete shear traction distribution as

$$q_x(x, y) = f_d\, p(x, y) - q_x^*(x, y)\ , \tag{4.7}$$

where $q_x^*(x, y)$ is a corrective distribution to be determined from the condition that the slip displacement (i.e. the relative tangential displacement) is zero in the stick area $\mathcal{A}_{\text{stick}}$. Conditions (4.3,4.7) require that $q_x^*(x, y)$ be non-zero only in $\mathcal{A}_{\text{stick}}$, and hence the stick condition defines a

well-posed boundary-value problem for $q_x^*(x,y)$. The inequality condition (4.4) precludes singularities in the shear tractions, and this imposes uniqueness on the solution for any given $Q_x < f_d\,P$. It is clear that the original Cattaneo-Mindlin solution (4.5) with $f = f_d$ satisfies these conditions, including the inequality, since in $\mathcal{A}_{\text{stick}}$, this would give $q_x(x,y) < f_d\,p(x,y) < f_s\,p(x,y)$.

4.2.3 Dependence on slip distance

The discussion so far is predicated on the assumption that as soon as stick is 'broken' there is an immediate transition to the dynamic coefficient f_d, but in practice we might expect a more continuous transition as slip occurs. We shall therefore examine the consequences of a friction law in which the coefficient of friction is a continuous and monotonic function $f(u)$ of the slip displacement u, such that

$$f(0) = f_s \quad \text{and} \quad f(u) \to f_d\ ; \quad u \to \infty\ . \tag{4.8}$$

Such a law can be regarded as a special case of the rate-state law ([17], [49]) and is also related to the the shear failure law proposed by Abercrombie and Rice [51]. Applications of similar laws to fault mechanics are discussed by Ben Zion [53].

In general, solutions of the corresponding contact problem will then require numerical solution, but it is instructive to consider some simple cases analytically. In particular, we shall consider the two-dimensional case where the bodies comprise a cylinder of radius R and a half space, so the contact pressure is given by

$$p(x) = \frac{E^*\sqrt{a^2 - x^2}}{2R}\ ; \quad P = \frac{\pi E^* a^2}{4R}\ , \tag{4.9}$$

where a is the semi-width of the contact area $-a < x < a$, and E^* is the composite elastic modulus [2].

We anticipate the existence of two symmetric slip regions $-a < x < -c$ and $c < x < a$ in which the slip displacement increases monotonically away from the stick-slip boundaries $x = \pm c$. Two limiting cases can also be identified. If $f(u)$ is a rather slowly decaying function of u, the friction coefficient will be close to f_s throughout the slip regions and the solution will approximate the constant coefficient case with $f = f_s$. At the other limit, if a very small amount of slip displacement is required to precipitate the change in coefficient, most of the slip area will be at or near f_d, but we must still allow for the existence of 'transition' regions $c < |x| < b$ in which $f > f_d$.

The exact form of the function $f(u)$ is not critical, but it is convenient to define a quantity W with the dimensions of surface energy through the relation

$$W = \int_0^\infty (f(u) - f_d) p\, du\ , \tag{4.10}$$

which is equivalent to the shear fracture energy defined by Abercrombie and Rice [51]. The contact pressure p will generally vary in the transition region, but if this is sufficiently short for p to be regarded as uniform, we can also define a length scale Δ characterizing the amount of slip needed to transition to dynamic friction, such that

$$\Delta = \frac{W}{(f_s - f_d)p} = \frac{1}{(f_s - f_d)} \int_0^\infty (f(u) - f_d)\, du\ . \tag{4.11}$$

Rabinowicz [45] conducted some simple but elegant experiments to determine f_s, f_d and Δ for metals, his results[1] being presented in Table 1.

[1] It is difficult to explain why different results might be obtained by simply interchanging the materials in the mild steel/copper case, but the difference is arguable within the range of likely experimental variance.

Materials	f_s	f_d	Δ (μm)
copper/mild steel	0.46	0.31	1
lead/mild steel	0.72	0.47	3
mild steel/copper	0.54	0.39	0.9
mild steel/titanium	0.63	0.45	6
mild steel/zinc	0.65	0.47	2

Table 1: Friction coefficients and slip length Δ for some metal combinations, from [45].

A special case satisfying equations (4.10, 4.11) is the step function $f = f_s - (f_s - f_d)H(u - \Delta)$, where $H(\cdot)$ is the Heaviside step function. The perceptive reader will notice a similarity here to Maugis' approximate formulation of the normal adhesive contact problem [54], where the adhesion law is also represented by a step function and the outer boundary of the adhered region is determined from the condition that the separation there is equal to a critical value. Indeed we shall see that there are significant mathematical analogies between the present problem and adhesive problems.

A double-Cattaneo-Mindlin solution

The present problem could be formulated using a step function for $f(u)$, but a simpler mathematical approximation can be obtained by adapting the 'double-Hertz' concept of Greenwood and Johnson [55]. We first note that the Cattaneo-Mindlin traction distribution $q_x(x) = q(x, a, c), Q_x = Q(a, c)$, where

$$q(x,a,c) = \sqrt{a^2 - x^2} - \sqrt{c^2 - x^2}\ ; \quad Q(a,c) = \frac{\pi(a^2 - c^2)}{2} \tag{4.12}$$

produces slip displacements $u_x(x)$, such that

$$\frac{\partial u_x}{\partial x} \equiv v(x,a,c) = 0\ ; \qquad -c < x < c \tag{4.13}$$

$$= -\frac{2\sqrt{x^2 - c^2}}{E^*} \qquad ;\ c < |x| < a \tag{4.14}$$

([2]), where the square roots in (4.12) are to be interpreted as zero in any region where their respective arguments are negative.

We next approximate the solution to the frictional problem as

$$q_x(x) = \frac{E^* f_d\, q(x,a,c)}{2R} + Cq(x,b,c)\ ; \quad Q_x = \frac{E^* f_d\, Q(a,c)}{2R} + CQ(b,c)\ , \tag{4.15}$$

where $c < b < a$. The corresponding slip displacements will then satisfy

$$\frac{\partial u_x}{\partial x}(x) = \frac{E^* f_d\, v(x,a,c)}{2R} + Cv(x,b,c)\ , \tag{4.16}$$

and this is zero in $-c < x < c$ from (4.13), showing that the stick condition can be satisfied by an appropriate rigid-body translation.

The shear tractions in $b < |x| < a$ are

$$q_x(x) = \frac{E^* f_d \sqrt{a^2 - x^2}}{2R} = f_d\, p(x)\ , \tag{4.17}$$

and hence satisfy the slip condition at $f = f_d$, since the other square-root terms make no contribution in this range. In $c < |x| < b$, the shear tractions are

$$q_x(x) = f_d\, p(x) + C\sqrt{b^2 - x^2}\ , \tag{4.18}$$

and we can choose the constant C so as to ensure that $q_x(c) = f_s\, p(c)$, giving

$$C = \frac{E^*(f_s - f_d)}{2R}\sqrt{\frac{a^2 - c^2}{b^2 - c^2}} \tag{4.19}$$

and

$$q_x(x) = \frac{E^* f_d\, q(x,a,c)}{2R} + \frac{E^*(f_s - f_d)}{2R}\sqrt{\frac{a^2 - c^2}{b^2 - c^2}}\, q(x,b,c)\ . \tag{4.20}$$

With this choice, the effective local coefficient of friction $f = q_x/p$ will decrease monotonically from f_s to f_d in $c < |x| < b$.

The final step is to determine the unknown radii c, b from the equilibrium condition $(4.15)_2$, and from (4.10) which we can write as

$$W = \int_c^b \left[q_x(x) - f_d\, p(x)\right] \frac{du_x}{dx} dx\ . \tag{4.21}$$

In $c < |x| < b$, we have

$$\frac{du_x}{dx} = -\frac{1}{R}\left(f_d + (f_s - f_d)\sqrt{\frac{a^2 - c^2}{b^2 - c^2}}\right)\sqrt{x^2 - c^2}\ , \tag{4.22}$$

from (4.14,4.19). Using this expression and (4.18) in (4.21) and evaluating the integral, we obtain

$$\begin{aligned} W = -\frac{E^* b(f_s - f_d)}{6R^2}\sqrt{\frac{a^2 - c^2}{b^2 - c^2}}\left(f_d + (f_s - f_d)\sqrt{\frac{a^2 - c^2}{b^2 - c^2}}\right) \\ \times \left[(b^2 + c^2)E(k) - 2c^2 K(k)\right]\ , \end{aligned} \tag{4.23}$$

where

$$k^2 = 1 - \frac{c^2}{b^2} \tag{4.24}$$

and

$$K(k) = \int_0^{\pi/2} \frac{d\theta}{\sqrt{1 - k^2 \sin^2\theta}}\ ; \quad E(k) = \int_0^{\pi/2} \sqrt{1 - k^2 \sin^2\theta}\, d\theta \tag{4.25}$$

are the complete elliptic integrals of the first and second kind respectively. The equilibrium condition is obtained from (4.12,4.15,4.19) as

$$Q_x = \frac{\pi E^*}{4R}\left[f_d(a^2 - c^2) + (f_s - f_d)\sqrt{(b^2 - c^2)(a^2 - c^2)}\right]\ . \tag{4.26}$$

If Q_x, W are given, (4.23, 4.26) provide two equations for the two unknown radii c, b.

The 'JKR' limit

If the transition from f_s to f_d occurs over a sufficiently small region, we can obtain a limiting solution analogous to the JKR solution of normal adhesion problems. We write $b = c + \delta$, where $\delta \ll c$, in which case (4.23) can be approximated as

$$W \approx \frac{\pi E^*(f_s - f_d)^2(a^2 - c^2)\delta}{16R^2} \quad \text{implying} \quad \delta \approx \frac{16R^2 W}{\pi E^*(f_s - f_d)^2(a^2 - c^2)}\ . \tag{4.27}$$

Also, the second term in $q_x(x)$ in equation (4.15) can be approximated as

$$Cq(x,b,c) \approx Cq(x,c,c) + C\delta\frac{\partial q}{\partial a}(x,c,c) = \frac{Cc\delta}{\sqrt{c^2 - x^2}}\ . \tag{4.28}$$

Applying the same approximation to equations (4.19, 4.26) and substituting for δ from (4.27), we obtain

$$q_x(x) \approx \frac{E^* f_d\, q(x,a,c)}{2R} + \sqrt{\frac{2WE^*c}{\pi(c^2-x^2)}}\,, \tag{4.29}$$

and

$$\frac{Q_x}{f_d P} = \frac{4RQ_x}{\pi E^* f_d a^2} \approx 1 - \frac{c^2}{a^2} + \frac{4R}{f_d\, a^2}\sqrt{\frac{2Wc}{\pi E^*}}\,. \tag{4.30}$$

Equation (4.29) defines a locally singular field, implying the existence of a mode II stress-intensity factor

$$K_{\rm II} \equiv \lim_{x\to c^-} q_x(x)\sqrt{2\pi(c-x)} = \sqrt{2WE^*}\,, \tag{4.31}$$

which is exactly analogous with the mode I stress intensity factor $K_{\rm I} = \sqrt{2\Delta\gamma E^*}$ in normal adhesion problems in the JKR limit, where $\Delta\gamma$ is the interface energy.

In an impressive series of experiments, Svetlizky and Fineberg [25] have observed frictional slip progressing by the relatively slow propagation of slip zones behind which the shear tractions approximate a square-root singularity. The strength of this singularity is approximately constant, indicating a well-defined value of fracture energy W, but they suggest it may depend on the local pressure, as a result of the area of actual contact being approximately proportional to pressure.

Ciavarella [56] presented solutions of contact problems with a mode II stress-intensity factor around the stick-slip boundary, motivated by Fineberg's observations. The present analysis shows that such an effect can be generated by a slip-dependent friction law of the form (4.8) and provides a rationale for determining an appropriate value of $K_{\rm II}$. In particular, we notice from (4.31) that the stress-intensity factor depends only on the composite modulus and W, and is otherwise independent of the details of the contact problem. Since *ex hypothesis*, the transition is assumed to occur over a small region (of width δ) in the contact area, we can assume that the contact pressure p is uniform in this region, and hence use the form (4.11) for W. This leads to a stress-intensity factor

$$K_{\rm II} = \sqrt{2E^*(f_s - f_d)p\Delta}\,, \tag{4.32}$$

which varies with $\sqrt{p}$ and is equivalent to the 'pressure-dependent toughness' criterion of Ciavarella [56].

Using (4.11) to recast equations (4.29, 4.30) in terms of Δ, we have

$$q_x(x) \approx \frac{E^* f_d\, q(x,a,c)}{2R} + E^*\sqrt{\frac{(f_s-f_d)\Delta c\sqrt{a^2-c^2}}{\pi R(c^2-x^2)}} \tag{4.33}$$

$$\frac{Q_x}{f_d P} \approx 1 - \frac{c^2}{a^2} + \frac{4}{f_d\, a^2}\sqrt{\frac{(f_s-f_d)R\Delta c\sqrt{a^2-c^2}}{\pi}}\,. \tag{4.34}$$

Small-scale transition zone

Equation (4.32) implies that at a sufficiently small distance s from the stick boundary, the frictional tractions have the singular form

$$q_x(s) \approx f_d p + \sqrt{\frac{E^*(f_s-f_d)p\Delta}{\pi s}}\,. \tag{4.35}$$

However, this expression violates the stick condition (4.4) in the region $0 < s < s_0$, where

$$\sqrt{\frac{E^*(f_s-f_d)p\Delta}{\pi s_0}} = (f_s - f_d)p \quad \text{or } s_0 = \frac{E^*\Delta}{\pi(f_s-f_d)p}\,. \tag{4.36}$$

An analogous situation is encountered in elastic-plastic fracture mechanics, where the 'small-scale yielding' criterion is used to determine whether the fields far outside the yield zone can reasonably be described by the elastic solution [57]. In the present case, the singular solution can be expected to give good results everywhere except very close to $x = c$, provided $s_0 \ll c$.

This criterion depends on c and hence on Q_x, but a rough estimate of the applicability of the JKR solution in the present problem can be obtained by using $p(0), a$ for p, c respectively, defining the modified criterion

$$\Lambda \equiv \frac{R\Delta}{(f_s - f_d)a^2} \ll 1 \,. \tag{4.37}$$

More general two-dimensional problems

We have analyzed the two-dimensional Hertzian problem in detail because the resulting expressions are algebraically straightforward, enabling the fundamental structure of the solution to be exposed. However, the same method can be applied to any two-dimensional problem involving a single symmetric contact area. We simply replace equation (4.12) by

$$q(x, a, c) = p(x, a) - p(x, c) \,; \quad Q(a, c) = P(a) - P(c) \,, \tag{4.38}$$

where $p(x, a)$ is the normal contact pressure when the contact area is defined by $-a < x < a$, and $P(a)$ is the corresponding normal force. We know from Ciavarella [8] and Jäger [52] that this will satisfy equation (4.13), so the traction distribution

$$q_x(x) = f_d q(x, a, c) - Cq(x, b, c) \tag{4.39}$$

will satisfy the stick conditions in $-c < x < c$ and the dynamic slip conditions in $b < |x| < a$. The rest of the solution can then be completed as in seen before.

If the length scale s_0 in (4.36) is sufficiently small to justify the JKR approximation, the second term will take the universal form (4.28), so the solution can be written down as the superposition of a conventional Cattaneo-Mindlin solution with coefficient of friction f_d and equation (4.28). In this context, it may be helpful to note that the limiting expression for $Q(b, c)$ is

$$Q(b, c) = \int_{-c}^{c} Cq(x, b, c)dx \to \sqrt{2\pi W E^* c} \,, \tag{4.40}$$

so the total tangential force is

$$Q_x = f_d \left[P(a) - P(c)\right] + \sqrt{2\pi W E^* c} \,. \tag{4.41}$$

Since Q_x will usually be prescribed, this provides an equation from which c can be determined as a function of Q_x.

4.2.4 Finite element results

The double Cattaneo-Mindlin solution is approximate in the sense that we are able to match a specific value of the fracture energy W or (equivalently) the length scale Δ, but the exact form of the function $f(u)$ cannot be prescribed. The implied form of this function depends on the dimensionless ratios $b/c, a/c$, some representative curves being shown as dashed and dotted lines in Fig. 4.1.

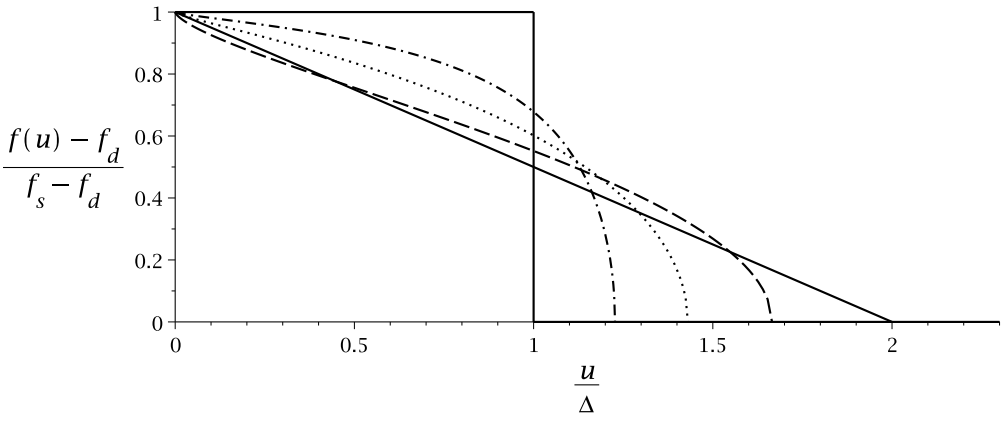

Fig. 4.1. The friction coefficient function $f(u)$ implied by the double Cattaneo-Mindlin solution for $a/c = 1.6, b/c = 1.5$ (━ · ━ · ━), $a/c = 8.0, b/c = 4.5$ (· · · ·), $a/c = 8.0, b/c = 1.2$ (━ ━ ━).

To assess the effect of this approximation, we constructed a finite element solution of the problem, as an extension of the "verification manual" VM272 example in Ansys 15 [58], which in turn is based on the method illustrated in [59] and an example given therein which compares satisfactorily with the analytical Cattaneo-Mindlin solution. It is based on a mortar formulation of the contact which is able to deal with nonconforming discretizations across boundaries and large sliding which is more than adequate for our problem. In [59], several examples and comparisons are made to show that this method has an optimal convergence rate and robustness with respect to other approaches. The example considers two parallel linear elastic half cylinders of radius R and pressed by a small distributed pressure on the diameter. A tangential pressure is then applied to cause friction at the contact interface, while the top of the upper cylinder is constrained from rotating. The bottom of the lower cylinder is fixed in all directions. The standard input listing available in ANSYS is adequate for many problems, but two minor changes made in the present case were:

1. We used quadratic PLANE183-CONTA172 instead of linear elements PLANE182-CONTA171, and we modified the mesh parametrically keeping the same ratio of elements, in order to improve marginally the accuracy of the results. For the figures reported in the paper we divided every element edge by 3 which brings the total number of elements to about 45000, but still permits a solution of an entire curve of loading in less than a minute.

2. We did not use the ANSYS variant of the friction law with just static and dynamic coefficients, since this does not permit a dependence on slip displacement. Instead, we defined a table of friction coefficients in terms of slip displacement.

Fig. 4.2 compares the shear traction $q_x(x)$ from equation (4.20) for $Q_x = 0.8 f_d P$, $f_s = 0.15, f_d = 0.1, \Lambda = 0.05$, with finite element results using the ramp (linear) function for $f(u)$ from Fig. 4.1. The agreement is clearly extremely good. Also shown on this figure are the conventional Cattaneo-Mindlin prediction (equivalent to taking $\Delta = 0$) and the JKR approximation (4.33). The latter gives good predictions everywhere except in the transition region, where of course the predicted singular stress is unphysical.

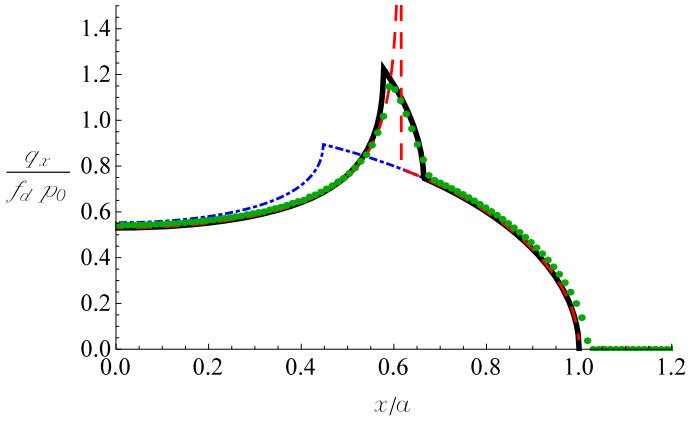

Fig. 4.2. Finite element results (●●●) for the shear traction distribution $q_x(x)$ for $Q_x = 0.8 f_d P$, $f_s = 0.15$, $f_d = 0.1$ and $\Lambda = 0.05$: ━━ Double Cattaneo-Mindlin solution (4.20), ━ · ━ · ━ Conventional Cattaneo-Mindlin solution (4.5) with $f = f_d$, ━ ━ ━ 'JKR' approximation of equation (4.33).

Fig. 4.3 shows a similar comparison for a larger value of Δ, so that the transition extends over a larger radius. In this figure, we compare equation (4.20) with finite element solutions using the ramp function and the step function respectively from Fig. 4.1. This figure shows that the traction distribution is relatively insensitive the the form of the function $f(u)$ for given values of $(f_s - f_d)$ and Δ, and hence that equation (4.20) can be expected to give good results for most practical slip-weakening laws.

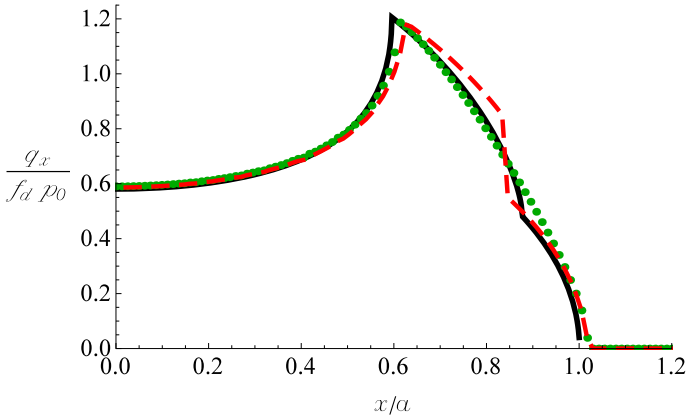

Fig. 4.3. Effect of the function $f(u)$ on the traction distribution $q_x(x)$: ●●● ramp (finite element), ━ ━ ━ step (finite element), ━━ equation (4.20). $Q_x = 0.9 f_d P$, $f_s = 0.15, f_d = 0.1, \Lambda = 0.277$.

4.2.5 Discussion

The principal new result from this analysis is that fracture mechanics concepts are introduced into the microslip problem, even when the friction law is merely an extension of the Coulomb law allowing differing static and dynamic coefficients. In particular, if the coefficient of friction varies with slip displacement over a relatively short slip distance Δ, we can determine a critical stress intensity factor or fracture toughness (4.32) that depends only on the static and dynamic coefficients, the form of the slip-weakening law, the composite modulus and the local contact pressure.

Equation (4.34) defines the relation between tangential force Q_x and the semi-length c of the stick area in the JKR limit, which is appropriate if the small-scale transition criterion $s_0 \ll c$ is satisfied. It is plotted in Fig. 4.4 for several values of the dimensionless parameter

$$\Psi = \left(\frac{f_s}{f_d} - 1\right) \frac{R\Delta}{f_d a^2} = \left(\frac{f_s}{f_d} - 1\right)^2 \Lambda \,. \tag{4.42}$$

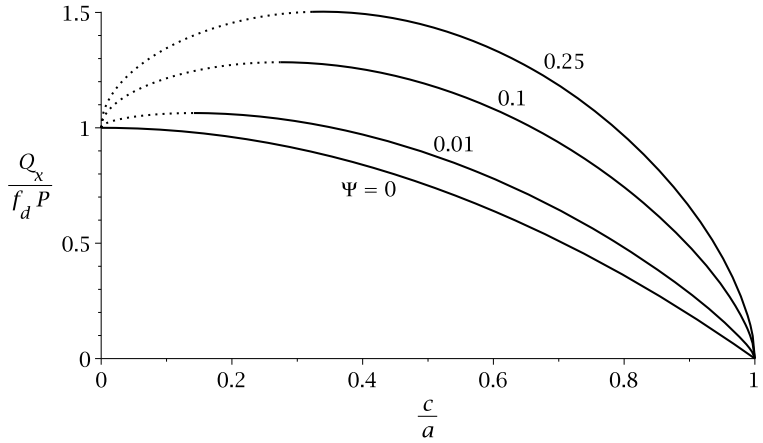

Fig. 4.4. The tangential force Q_x as a function of the radius c of the stick zone (JKR limit).

All the curves except the limiting case $\Psi = 0$ exhibit a maximum $Q_x = Q_{\max}$ at a non-zero value of c, implying that under tangential force control, the system would jump unstably to full sliding once this maximum is reached. The unstable range is shown dotted in Fig. 4.4.

Similar plots were made for the double Cattaneo-Mindlin solution, using equations (4.26, 4.23) with $W = (f_s - f_p)\Delta$. Fig. 4.5 compares the resulting curves for $\psi = 0.1$ and $\Lambda = 0.025, 0.4$ with the JKR solution. Notice that changing Λ at constant ψ implies a change in the friction coefficient ratio f_s/f_d. The truncation in these curves near $c = a$ occurs because the outer boundary b of the transition region cannot exceed the boundary a of the contact area. When $b = a$, the double Cattaneo-Mindlin solution reduces to a conventional Cattaneo-Mindlin solution with $f = f_s$, so we have arbitrarily used this result to continue the curves to $c = a$ [shown dotted].

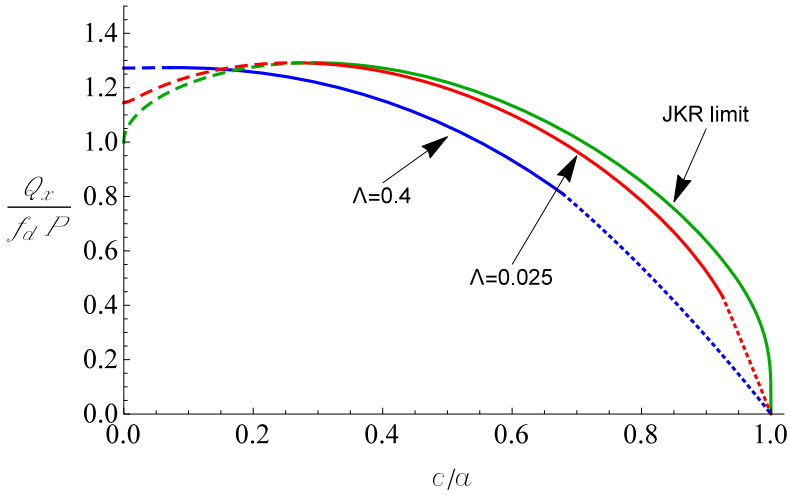

Fig. 4.5. Comparison of the double Cattaneo-Mindlin solution with the JKR limit for $\psi = 0.1$.

As predicted, the curve for $\Lambda = 0.025$ is very close to the JKR curve, though the maximum Q_x is shifted slightly to the left. Notice incidentally that we might have chosen to plot the double Cattaneo-Mindlin curves as functions of the location of the mid-point $(c + b)/2a$ of the slip-stick transition region, in which case this shift would be much reduced. For larger Λ, the maximum occurs at significantly lower values of c, but $Q_{\max}$ is still very well predicted by the JKR theory even for $\Lambda = 0.4$.

Experimental measurements of static friction coefficient are usually obtained by increasing the applied tangential force until sliding commences. However, it is clear that under these circumstances, microslip is likely to occur before gross sliding commences, and hence in the present geometry such experiments would lead to the static coefficient of friction being identified as $Q_{\max}/P$, which generally differs from f_s.

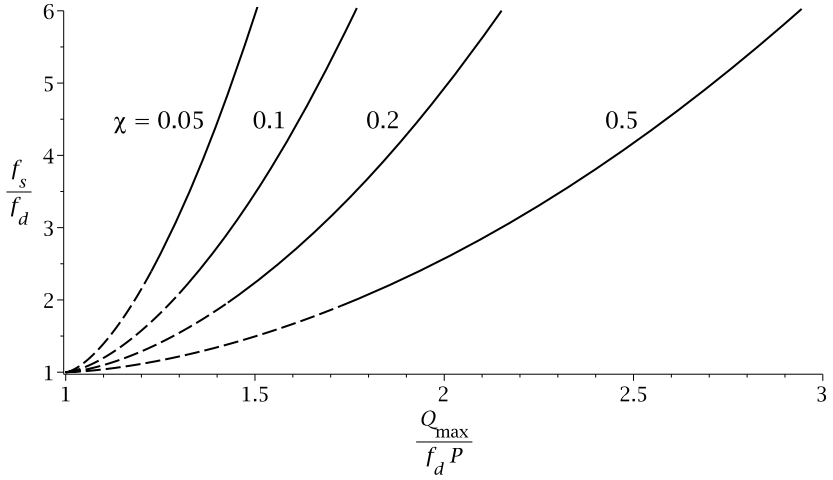

Fig. 4.6. The coefficient ratio f_s/f_d as a function of the apparent ratio $Q_{\max}/f_d\,P$.

Fig. 4.6 shows the relationship between f_s/f_d and the 'apparent' value of this ratio determined as $Q_{\max}/f_d\,P$, for various values of

$$\chi = \frac{R\Delta}{f_d a^2} = \left(\frac{f_s}{f_d} - 1\right)\Lambda\,. \tag{4.43}$$

The dashed lines in this figure correspond to ranges in which the small-scale transition criterion $s_0 \ll c$ is not satisfied. We notice that the apparent static friction coefficient is always significantly lower than f_s. The reason of course is that by the time $Q_{\max}$ is reached, a significant part of the contact area has slipped sufficiently to transition to a local coefficient f_d, and the measured coefficient is a weighted average over the whole contact area.

Notice that the limiting case $\chi = 0$ can arise only if $\Delta = 0$, meaning that the transition from f_s to f_d occurs over an infinitesimal slip distance. As explained in §4.1.2, the partial slip solution is then identical to the conventional Cattaneo-Mindlin solution with $f = f_d$ and hence slip occurs for $Q = f_d P$ regardless of the static coefficient of friction f_s. This case is defined by the vertical axis in Fig. 4.6.

4.3 Conclusions

We have shown that the use of a slip-weakening friction law has a qualitative effect on the solution of microslip problems. The mechanics of the classical Cattaneo-Mindlin problem then have a mathematical structure similar to that of the adhesive contact problem, and we can identify an

analogue of the 'JKR' solution, in which the extent of the stick zone is governed by the occurrence of a pressure-dependent mode II stress-intensity factor at the stick-slip boundary. By exploring the two-dimensional Hertzian geometry, we were able to identify the equivalent fracture toughness, which is independent of the detailed geometry, but proportional to the square root of the local contact pressure. We also defined a length scale s_0 analogous to the small-scale yielding criterion whose value enables us to judge whether the singular solution gives a good approximation to the more exact solution.

The tangential force reaches a maximum before the stick zone has shrunk to zero, at which point there will be a discontinuous change of state to gross sliding. This implies that estimates of the static coefficient of friction from experiments on the inception of sliding will generally significantly underestimate the values appropriate at the microscale.

Chapter 5

Partial slip solutions with Griffith friction

In the previous chapter we analyzed the microslip problem between bodies when a friction law, more refined that the classical Coulomb law, is used. In particular we considered a slip weakening friction law which implies a transition zone where the friction coefficient $f(u)$ decays from the static f_s to the dynamic f_d value. It was shown that for vanishingly small length of the transition zone a "JKR" approximation can be used where the shear traction distribution is singular on the transition line. In this limit the microslip problem is governed by the fracture energy W, and a "Griffith friction model" is defined. In this chapter we will use this Griffith friction to solve the partial slip problem for power law and sinusoidal profiles.

5.1 Introduction

Rabinowicz, in 1951, [45] had conducted experiments to determine the transition between static and kinetic conditions for metal surfaces, measuring the energy that has to be given to one of the bodies to start it moving by using inclined planes with an angle insufficient to start sliding statically, but large enough to initiate slip by impacting a small mass. In his case with various metal surfaces, he found a static coefficient "f_s" persisting for distances "d_c" of the order of μm, and gradually decaying to the kinetic coefficient "f "(see Table 1). Specifically, we can define a frictional "fracture energy" per unit surface

$$W_{slip} = \int_0^{+\infty} (f(u) - f) p du \tag{5.1}$$

where $f(u)$ is the function that relates the coefficient of friction with the slip distance "u" and p is the local pressure. The product $(f_s - f)\, d_c$ in Table 1 gives a rough idea of the fracture energy for a given pressure, which we cannot estimate from Rabinowicz' paper. Slip-weakening friction laws have been introduced in fault mechanics of earthquakes, which relate inception of slip to concepts of fracture mechanics: Ida [60] and Palmer and Rice [61] have been the pioneer in this field, but fracture mechanics is now an established framework for earthquake friction ([62],[63],[53]), although experimental evidence may have been obtained firstly by Svetlizky and Fineberg [25] following a series of interesting experiments by the group of Jay Fineberg ([19],[22],[23],[24],[20]). Fineberg's group measured a number of effects with accuracy, including the fact that the ratio between shear and normal stresses along the interface can locally far exceed (a ratio of about 4 to 6) the static friction coefficient without precipitating slip ([22],[23]), pointing to fracture mechanics singular shear tractions, as proved more precisely in Svetlizky and Fineberg [25]. In general, this ratio is

correlated to the speed of propagating fronts, but known mode II field seem to correlate well at all speeds, except perhaps the very fast propagation speeds — however, these dynamic effects cannot be taken into account in a quasi-static model as we're going to advance here. The "fracture energy" as is called by Palmer and Rice [61], or critical energy for propagation, is a constant in Fineberg's experiments within the accuracy of experimental evidence, although they suggest it may depend only on the local pressure, based on an argument on the effective friction dissipation scaling with the bulk toughness via the real contact area reduction of the nominal interface area. Notice that the two areas of research, that initiated by Rabinowicz [45] with the experiments with sliding metals, with that of geophysics, are largely separated and have not been used in connection one with the other. This may be because in metals the difference between static and dynamic friction is small, as also mentioned by Richard Feynman in his famous lectures [46], and in agreement with the data of Table 1. Instead, in fault mechanics [47] the ratio is estimated to be of the order of a factor 10, and cause the definition "strong but brittle" fault [48]; "strong" because of the high peak static shear stress but "brittle" because of the low residual shear stress. In the data collected

in Table 2 and extracted in turn from a variety of reliable sources, it seems that values similar to those in geophysics can be obtained with brittle materials, although the reason for this behavior requires further investigation.

pair #	Material 1	Material 2	f_s	f	f_s/f	$d_c\,[\mu m]$	$(f_s - f)\,d_c\,[\mu m]$
1	copper	mild steel	0.46	0.31	1.484	1	0.15
2	lead	mild steel	0.72	0.47	1.532	3	0.75
3	Mild steel	copper	0.54	0.39	1.385	0.9	0.135
4	Mild steel	titanium	0.63	0.45	1. 4	6	1.08
5	Mild steel	zinc	0.65	0.47	1.383	2	0.36

Table 1. From [45]. Values of static coefficient of friction, kinetic coefficient of friction, the characteristic distance for which static coefficient of friction f_s drops to kinetic coefficient of friction f, the ratio f_s/f and an estimated value of "fracture energy" normalized by the local pressure (which is expected to be equal in all tests, but is not reported).

pair #	Material 1	Material 2	f_s	f	f_s/f
1	Cast Iron	Cast Iron	1,1	0,15	7,33
2	Zinc	Cast Iron	0,85	0,21	4,05
3	Copper	Cast Iron	1,05	0,29	3,62
4	Glass	Glass	0,95	0,4	2,38
5	Steel(Hard)	Steel (Hard)	0,78	0,42	1,86
6	Steel (Mild)	Steel (Mild)	0,74	0,57	1,30
7	Steel (Mild)	Lead	0,95	0,95	1,00
8	Aluminum	Aluminum	1,2	1,4	0,86

Table 2. Data for the static coefficient of friction f_s , kinetic coefficient of friction f, and their ratio f_s/f reordered and taken from the list compiled by the late Roy Beardmore using a variety of handbooks listed in his web site[1]

Since PMMA in the data obtained by Fineberg's group shows a ratio of static to kinetic friction coefficient up to 6, this behaviour seems to correspond to the class of "strong but brittle" interfaces as Rice [48] defines them, and indeed we also notice that other materials commonly believed to be "brittle" seem to behave similarly as from the data in Table 2 for Cast Iron vs either Cast Iron but also Zinc and Copper. It is with these cases in mind that we developed a Griffith theory of inception of slip in [56], limited to Hertzian 3D geometry, whereas here we shall consider a general

[1] http://www.roymech.co.uk/Useful_Tables/Tribology/co_of_frict.htm#coef

2D geometry and examine in details the effect of geometry for a few cases of interest. We report, for completeness, that in some cases (as Al on Al in Table 2), an inverse behavior is reported, with an increment of friction coefficient when sliding, and some models do show how kinetic friction can be greater than static friction [64], which would require different modelling strategies.

5.2 Theoretical analysis

5.2.1 Cattaneo-Mindlin solution

For the classical basic case in plane geometry (see Fig. 5.1), the main results of the classical Cattaneo problem are given in the first chapter and a much deeper analysis can be found in a number of textbooks, from Hills et al. [1], to Johnson [2], Barber [39], and Popov and Hess [65]. In the standard CM problem, we usually write the Coulomb friction condition, i.e. that shearing traction must be less than the limiting value in S_{stick}, i.e.[2]

$$|q(x)| < -fp(x), \qquad x \in S_{stick}. \tag{5.2}$$

but here, in analogy with what suggested by Ciavarella [56] for the 3D axisymmetric purely Hertzian case, we are going to define an "energetic criterion" (or a "Griffith" friction condition) as a condition that defines the boundary between the stick and the slip zone. This will yield the shear traction to be singular with an imposed strength of the singularity, as it is customary in the Linear Elastic Fracture Mechanics (LEFM) of proper cracks. Similarly to LEFM, we propose here a solution involving in principle infinite shear, and not for example the more complete one assuming a finite static friction (which corresponds to a cohesive model in fracture) as described in [38]. In particular, as LEFM gives the conditions of small-scale yielding to occur, so does Papangelo et al. [38] for the solution involving theoretically infinite friction to be valid.

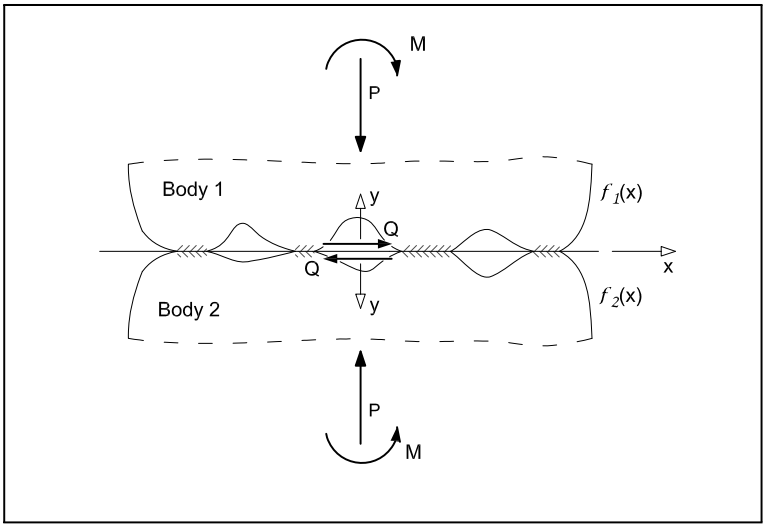

Figure 5.1. Basic set-up considered in the analysis

We seek solutions for contacts with "infinite" friction, where slip occurs at the edge of each contact area, but the shearing traction distribution can be defined initially in the same manner as the standard Cattaneo-Mindlin solution, as a correction of the full sliding term in the stick zone,

[2] Note that the negative sign in due to our convention $p(x) = \sigma_{yy}(x, 0)$.

of dimension and location presently unknown, which we denominate $q^*(x) = fp^*(x)$. Hence, for $Q < 0$, without loss of generality, one has

$$q(x) = \begin{cases} fp(x) + q^*(x), & x \in S_{stick} \\ fp(x), & x \in S_{slip} \end{cases} \tag{5.3}$$

Then, the integral equation for relative displacements in the tangential direction states, using $g_0'(x) = 0$, and substituting (1.49) for the full sliding component, becomes

$$0 = \frac{1}{\pi} \int_S \frac{q(t)\,dt}{x-t} = \frac{E^* f}{2} h'(x) + \frac{1}{\pi} \int_{S_{stick}} \frac{q^*(t)\,dt}{x-t}, \qquad x \in S_{stick} \tag{5.4}$$

where E^* is the composite modulus, $q^*(x) = 0$ in the slip zones, by definition, and in the stick zone, $q^*(x)$ is the solution of the following integral equation

$$\frac{1}{\pi} \int_{S_{stick}} \frac{-q^*(t)/f}{x-t} dt = \frac{E^*}{2} h'(x), \qquad x \in S_{stick} \tag{5.5}$$

which we can recognize as being of exactly the same form as the original equation for normal contact for $\beta = 0$, eq.(1.49) (with $p(x)$ replaced by $-q^*(x)/f$, and the domain of the integral suitably scaled). However, contrary to the standard CM case, where we don't admit solutions being unbounded at the edges of the stick zone [8], here we shall permit this variant. We recognize therefore the problem in the stick zone for the corrective shear as being equivalent to that of JKR solution for the shape of the punch interested by the stick zone, where JKR is the classical solution for the normal contact problem in the presence of adhesion [66]. It should be borne in mind, however, that we are not dealing with the presence of adhesion, as on the contrary, we assume that classical adhesive-less conditions apply in the normal contact problem.

5.2.2 The JKR solution for plane problems

Here the JKR solution for a general plane problem is derived, which we shall later use as a corrective solution for the full sliding component of the tangential contact problem. If the contact area is not symmetrical with respect to the origin, say $-a + \delta \le x \le a + \delta$, on assuming $t = \tau + \delta, x = \xi + \delta$, the integral equation (1.49) for the pressure distribution becomes

$$\frac{E^*}{2} h'(\xi + \delta) = \frac{1}{\pi} \int_{-a}^{a} \frac{p(\tau + \delta)\,d\tau}{\xi - \tau}, \qquad -a \le \xi \le a \tag{5.6}$$

where a is the semi-dimension of the contact area, and δ is the offset with respect to the origin of coordinates $x = 0$, in which the function $h(x)$ is defined by eq.(1.49). The solution for the corrective shear traction in the stick zone is equivalent to a JKR solution for a plane geometry. We therefore use the case of a general profile in contact over the range $-a \le \xi \le a$ (see [8])

$$p(\xi + \delta) = -\frac{E^*}{2\pi\sqrt{a^2 - \xi^2}} \int_{-a}^{a} \frac{h'(\tau + \delta)\sqrt{a^2 - \tau^2}\,d\tau}{\xi - \tau} - \frac{1}{\pi} \frac{P}{\sqrt{a^2 - \xi^2}}, \qquad -a \le \xi \le a \tag{5.7}$$

(notice that a positive load induces a negative, i.e. compressive, pressure) together with the condition now on the Stress Intensity Factor (SIF)

$$K_I = \lim_{\xi \to a} \sqrt{2\pi(a - \xi)}\, p(\xi + \delta) = K_{Ic} \tag{5.8}$$

To determine the moment in the case of non-symmetrical punch, we would additionally impose the condition to have equal SIFs at the two ends. The usual CM solution is obtained back when $K_{Ic} = 0$. Equation (5.7) can be separated in the adhesive (subscript "A") and adhesiveless (subscript "AL") contribution

$$p(\xi+\delta) = p_{AL}(\xi+\delta) + p_A(\xi+\delta), \qquad -a \le \xi \le a \tag{5.9}$$

$$P = P_{AL} - P_A \tag{5.10}$$

where

$$P = -\int_{-a+\delta}^{a+\delta} p(t)\,dt, \qquad P_{AL} = -\int_{-a+\delta}^{a+\delta} p_{AL}(t)\,dt, \qquad P_A = \int_{-a+\delta}^{a+\delta} p_A(t)\,dt \tag{5.11}$$

Eq. (5.7) for $p(\xi+\delta)$ is rewritten imposing the adhesiveless contribution to be bounded at the extremes (in particular $p_{AL}(\xi = \pm a) = 0$),

$$p_{AL}(\xi+\delta) = -\frac{E^*}{2\pi}\sqrt{a^2-\xi^2}\int_{-a}^{a} \frac{h'(\tau+\delta)\,d\tau}{\sqrt{a^2-\tau^2}(\tau-\xi)}, \qquad -a \le \xi \le a \tag{5.12}$$

$$p_A(\xi+\delta) = \frac{1}{\pi}\frac{P_A}{\sqrt{a^2-\xi^2}}, \qquad -a \le \xi \le a \tag{5.13}$$

with the further side conditions (see [8])

$$\int_{-a}^{a} \frac{h'(\tau+\delta)\,d\tau}{\sqrt{a^2-\tau^2}} = 0, \qquad P_{AL} = -\frac{E^*}{2}\int_{-a}^{a} \frac{h'(\tau+\delta)\,\tau d\tau}{\sqrt{a^2-\tau^2}} \tag{5.14}$$

To determine the moment M, assuming the flat punch solution is symmetrical (because the K_I will not be different on the two sides of the contact), rotational equilibrium is unaffected, and this gives the additional equation in terms of the adhesive-less pressure only

$$\begin{aligned} M &= -\int_{-a+\delta}^{a+\delta} p(t)\,tdt = -\int_{-a+\delta}^{a+\delta} p_{AL}(t)\,tdt = -\int_{-a}^{a} p_{AL}(\tau+\delta)(\tau+\delta)\,d\tau \\ &= P_{AL}\delta - \int_{-a}^{a} p_{AL}(\tau+\delta)\,\tau d\tau = P_{AL}\delta + \frac{1}{A}\int_{-a}^{a} h'(\tau+\delta)\sqrt{a^2-\tau^2}d\tau \end{aligned} \tag{5.15}$$

In particular, all the solutions shown in (see [8],[10]) can be used in this context as solutions for the term p_{AL}, P_{AL}. Moving to the new solution of the partial slip Cattaneo problem is therefore routine, since the side condition on K_I can now be written due to P_A alone,

$$K_I = \lim_{\xi\to a}\sqrt{2\pi(a-\xi)}p(\xi+\delta) = \frac{P_A}{\sqrt{\pi a}} \tag{5.16}$$

which leads to

$$P_A = K_{Ic}\sqrt{\pi a} \tag{5.17}$$

or in terms of a critical energy release rate $W = \frac{K_{Ic}^2}{2E^*}$. Hence, in general we can write

$$P = P_{AL} - \sqrt{2\pi E^* a W} \tag{5.18}$$

where for the Hertzian geometry we have

$$P_{AL} = P_H = \frac{\pi E^* a^2}{4R} \tag{5.19}$$

The pull-off force per unit length is the minimum of (5.18). Equating to 0 the first derivative of (5.18) with respect to a the critical size of the contact area a_c is found

$$a_c = R\left(\frac{2W}{\pi E^* R}\right)^{1/3} \tag{5.20}$$

Substituting the latter result into (5.18) the pull-off force is obtained

$$P_{\min} = \frac{3}{4}\left(4\pi E^* W^2 R\right)^{1/3} \tag{5.21}$$

Notice the weak dependence on elastic modulus, which is not present in the 3D version of the JKR solution.

For the non simply-connected contact areas, it is clear that the general procedure indicated here, that of superposing flat punch solutions to the bounded-bounded adhesiveless solutions, works equally well, as used for example in the case of a sinusoidal profile in [67].

As a consequence of the analogy established, the corrective load to the full sliding tangential contact will be given by noting that, according to eq.(5.5)

$$\frac{|Q^*|}{f} = P^* \tag{5.22}$$

where the corrective normal load is is given by (5.18) on which we apply the superscript "*" to identify this as a corrective tangential contact solution which in turn is composed by two contributions

$$P^* = P^*_{AL} - \sqrt{2\pi E^* c W} \tag{5.23}$$

and c is the half-width of the stick zone. It should be borne in mind that, with respect to the definition (5.1), the fracture energy to use in the corrective problem should consider the way the corrective problem is defined. In [38], it was shown that in a more refined cohesive model involving slip-weakening friction laws, when the transition from static to dynamic coefficient of friction takes place over a sufficiently small slip distance, the shear traction distribution tends to a JKR singular solution. However, the equivalence of the results is obtained for

$$W = \frac{1}{f^2}\int_0^{+\infty} (f(u) - f) p du \tag{5.24}$$

The stick zone is $-c + \delta^* \le x \le c + \delta^*$, and so let us define $t = \tau + \delta^*, x = \eta + \delta^*$. Hence, the corrective solution in the stick zone is given by the two contributions: an "adhesiveless" contribution to the corrective tractions (5.12) $q\left(\eta + \delta^*\right) = q_{AL}\left(\eta + \delta^*\right) + q_A\left(\eta + \delta^*\right)$, where

$$-q^*_{AL}\left(\eta + \delta^*\right)/f = \frac{E^*}{2\pi}\sqrt{c^2 - \eta^2}\int_{-c}^{c} \frac{h'\left(\tau + \delta^*\right) d\tau}{\sqrt{c^2 - \tau^2}\left(\tau - \eta\right)}, \qquad -c \le \eta \le c \tag{5.25}$$

$$-q^*_{A}\left(\eta + \delta^*\right)/f = \frac{1}{\pi}\frac{P^*_A}{\sqrt{c^2 - \eta^2}}, \qquad -c \le \eta \le c \tag{5.26}$$

The conditions $q^*_{AL}\left(\eta = \pm c\right) = 0$, and equilibrium translate into the following two equations

$$\int_{-c}^{c} \frac{h'\left(\tau + \delta^*\right) d\tau}{\sqrt{c^2 - \tau^2}} = 0, \qquad -Q^*_{AL}/f = -\frac{E^*}{2}\int_{-c}^{c} \frac{h'\left(\tau + \delta^*\right)\tau d\tau}{\sqrt{c^2 - \tau^2}} \tag{5.27}$$

These equations give the offset δ^*, and the size of the stick zone c. Note that, for a non-symmetrical self-similar profile (i.e. the functions on the right and the left of the $x = 0$ axes are each self-similar) the offset of contact area, and offset of stick zone are proportional, i.e. $\delta/\delta^* = c/a$, as the rotation is fixed. The tangential load may be calculated from

$$|Q| = fP - \left[\frac{fE^*}{2} \int_{-c}^{c} \frac{h'(\tau + \delta^*)\,\tau d\tau}{\sqrt{c^2 - \tau^2}} - f\sqrt{2\pi E^* cW} \right] \tag{5.28}$$

If we divide by fP (where P is the true normal load, obviously from the adhesiveless solution), and we define as in [8]

$$\Phi(x, y) = \int_{-x}^{x} \frac{h'(t + y)\,tdt}{\sqrt{x^2 - t^2}}. \tag{5.29}$$

then $\frac{|Q|}{fP}$, which ranges from 0 to 1 for full sliding in the original CM theory as $\frac{|Q|}{fP} = 1 - \frac{\Phi(c,\delta^*)}{\Phi(a,\delta)}$, is here changed into

$$\frac{|Q|}{fP} = 1 - \left[\frac{\Phi(c, \delta^*) - 2\sqrt{\frac{2\pi cW}{E^*}}}{\Phi(a, \delta)} \right] \tag{5.30}$$

5.3 Solution for partial slip contact

5.3.1 Hertzian case

Starting with the Hertzian case, in the usual parabolic approximation is $h'(x) = x/R$, where R is the radius of the cylindrical punch, and the stick zone is centrally positioned and is of half-width c. The dimensionless normalized shearing force ($|Q|/fP$), as a function of the size of the stick zone (c/a), is found using (5.28) and the Hertzian equation $P_H = \frac{\pi E^* a^2}{4R}$

$$\frac{|Q|}{fP} = 1 - \left[\frac{\frac{\pi c^2}{2R} - 2\sqrt{\frac{2\pi cW}{E^*}}}{\frac{\pi a^2}{2R}} \right] \tag{5.31}$$

but it is convenient to rewrite the adhesion-related term by deriving the "critical size" for the stick zone size as c_c which makes eq. (5.31) maximum, writing

$$\frac{d}{dc}\left(\frac{|Q|}{fP}\right) = \frac{2R}{\pi a^2}\left(-\frac{\pi c}{R} + \sqrt{\frac{2\pi W}{E^* c}}\right) = 0 \tag{5.32}$$

which results in

$$c_c = R\left(\frac{2W}{\pi E^* R}\right)^{1/3} \tag{5.33}$$

and which makes $\frac{|Q|}{fP}$ a maximum.

Hence[3] eq. (5.31) can be rewritten as

$$\frac{|Q|}{fP} = 1 - \left(\frac{c}{a}\right)^2 \left[1 - 4\left(\frac{c_c}{a}\frac{a}{c}\right)^{3/2}\right] \tag{5.35}$$

[3] To have a term of comparison, the 3D Hertzian case leads to [56]

$$\frac{Q}{fP} = 1 - \left(\frac{c}{a}\right)^3 \left[1 - 2\left(\frac{c_c}{a}\frac{a}{c}\right)^{3/2}\right] \tag{5.34}$$

which is quite similar in form, and therefore we expect the same type of results.

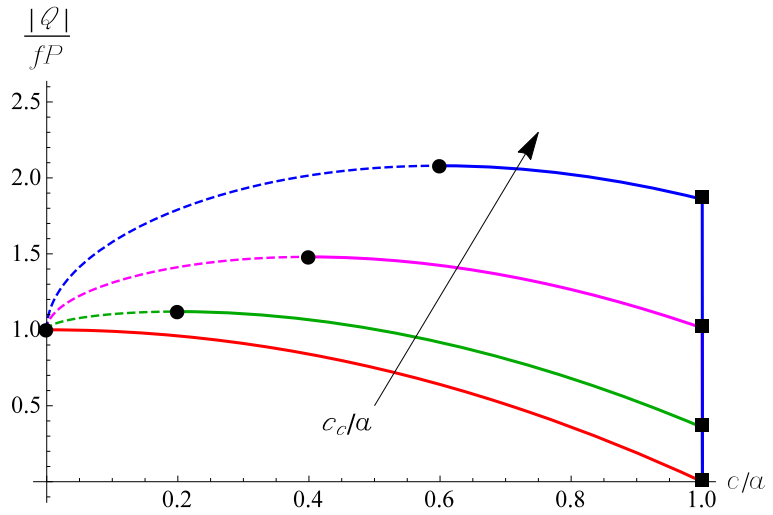

Figure 5.2. $|Q|/fP$ for Hertzian contact plotted against the dimensionless width of the stick zone c/a, for different values of the ratio $c_c/a = [0 - 0.2 - 0.4 - 0.6]$. For each curve the minimum $|Q|/fP$ at which partial slip commences is indicated with a black square, while the maximum value of the stable branch is indicated with a black circle.

In Fig. 5.2 we plot the ratio $|Q|/fP$ as a function of the dimensionless width of the stick zone c/a, for different values of the ratio $c_c/a = [0 - 0.2 - 0.4 - 0.6]$ which corresponds to higher and higher fracture energy in the transition from stick to slip. For $c_c/a = 0$ the classical CM solution is retrieved where the maximum shear force ($|Q|/fP = 1$) is obtained at $c/a = 0$. For $c_c/a > 0$ it is seen that no sliding begins until we reach a critical tangential load, after which the stick zone decreases up to a certain minimum size, corresponding to a maximum tangential load. Turning back to the minimum load needed to trigger a partial slip condition, this can be easily estimated putting $(c/a) = 1$ in (5.35),

$$\left(\frac{|Q|}{fP}\right)_{\min} = 1 - \left(1 - 4\left(\frac{c_c}{a}\right)^{3/2}\right) = 4\left(\frac{c_c}{a}\right)^{3/2} \tag{5.36}$$

When $\left(\frac{|Q|}{fP}\right)_{\max}$ is reached, the curves become unstable under load control (hence, we plot them as dashed curves), with a sudden decrease of c to 0. Notice that $\left(\frac{|Q|}{fP}\right)_{\max}$ can be even interpreted as the ratio between the apparent static friction coefficient measured during an experiment, and the dynamic one, which is both the local value in the slip zones, and the global friction coefficient measured under gross sliding conditions. The maximum $\left(\frac{|Q|}{fP}\right)_{\max}$ can be obtained using (5.32),

$$\left(\frac{|Q|}{fP}\right)_{\max} = 1 + 3\left(\frac{c_c}{a}\right)^2 = 1 + 3\left[\frac{1}{4}\left(\frac{|Q|}{fP}\right)_{\min}\right]^{4/3} \tag{5.37}$$

and the highest increase is $\left(\frac{|Q|}{fP}\right)_{\max} = 4$ which is double of the highest increase obtained in 3D [56]. In Fig. 5.3, we plot the maximum and the minimum value of the $\left(\frac{|Q|}{fP}\right)$ as a function of $\frac{c_c}{a}$. Notice that increasing the fracture energy, both the maximum and the minimum shear force increase and for $\frac{c_c}{a} = 1$ we have $\left(\frac{|Q|}{fP}\right)_{\min} = \left(\frac{|Q|}{fP}\right)_{\max}$.

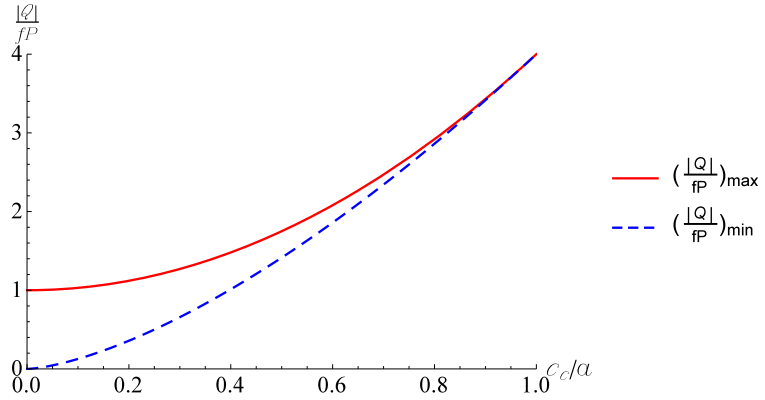

Figure 5.3. Maximum and minimum values of the ratio $\frac{Q}{fP}$ for Hertzian contact as a function of the dimensionless critical size of the stick area c_c/a.

Shear tractions

For the Hertzian case, in the stick zone we have

$$q(x) = fp(x) + fp^*(x) = \tag{5.38}$$

$$= f\left[-p_0\sqrt{1-\left(\frac{x}{a}\right)^2} + \left(p_0^*\sqrt{1-\left(\frac{x}{c}\right)^2} - \frac{p_0'}{\sqrt{1-\left(\frac{x}{c}\right)^2}}\right)\right] \tag{5.39}$$

where $p_0' = \sqrt{\frac{2E^*W}{\pi c}}, p_0^* = \frac{E^* c}{2R}, p_0 = \frac{E^* a}{2R}$ and

$$\frac{p_0^*}{p_0} = \frac{c}{a}, \qquad \frac{p_0'}{p_0} = 2\left(\frac{c_c}{a}\right)^{3/2}\left(\frac{a}{c}\right)^{1/2} \tag{5.40}$$

Thus the dimensionless shear tractions are

$$\frac{q}{-fp_0} = \sqrt{1-\left(\frac{x}{a}\right)^2} - \frac{c}{a}\sqrt{1-\left(\frac{x}{c}\right)^2} + \frac{2\left(\frac{c_c}{a}\right)^{3/2}\left(\frac{a}{c}\right)^{1/2}}{\sqrt{1-\left(\frac{x}{c}\right)^2}} \tag{5.41}$$

In Fig. 5.4 (a) we plot (5.41) as a function of x/a for a fixed value of $c_c/a = 0.2$ and for different radius of the stick zone $c/a = [0.2 - 0.4 - 0.6 - 0.8]$. Notice that with this choice of c_c/a, the red dashed curve coincides with the last stable solution. In Fig. 5.4 (b) we plot (5.41) for a given stick radius $c = 0.6$ and different critical radius of the stick zone $c_c/a = [0 - 0.1 - 0.2 - 0.3 - 0.4]$. It is seen that increasing the transition energy a stronger strength of the singularity is obtained which also leads to obtain higher load in the stick zone. This behavior is responsible of the increasing of the apparent friction coefficient that appears in Fig. 5.2.

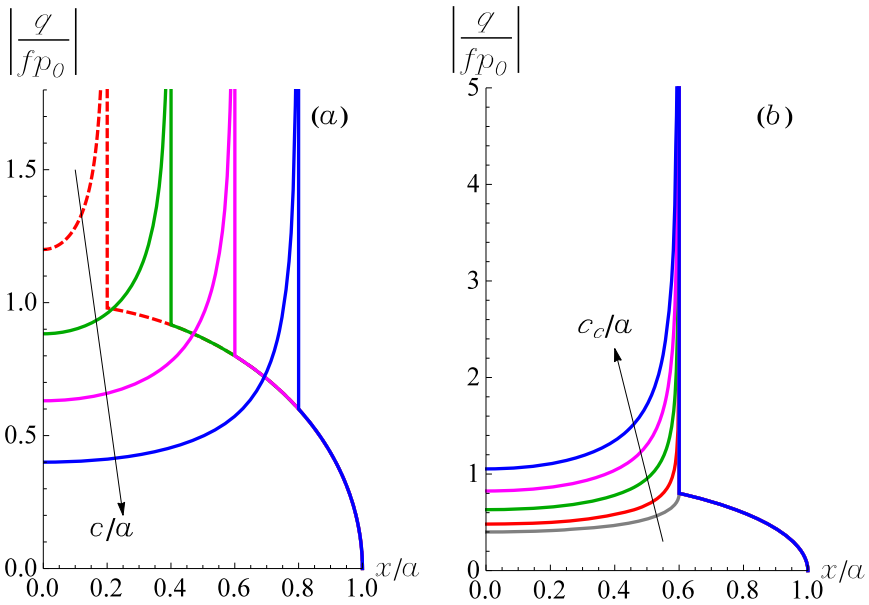

Figure 5.4. Hertzian case (a) Shear tractions for a given $c_c/a = 0.2$ (read transition energy) and different stick radius $c/a = [0.2 - 0.4 - 0.6 - 0.8]$.(b) Shear tractions for a given $c/a = 0.6$ and different critical radius of the stick zone $c_c/a = [0 - 0.1 - 0.2 - 0.3 - 0.4]$.

5.3.2 Power-law punches

This case is useful in view of considering deviations from Hertzian geometry. Consider a punch of power-law profile $f_1(x) = C|x|^k$, including polynomial of any order, in contact with a half-plane. The function $h(x)$ is defined by

$$h'(x) = -\text{sign}(x)\, Ck\, |x|^{k-1}. \tag{5.42}$$

one obtains (see App.I of [10] for details)

$$P = Cka^k E^* \frac{\sqrt{\pi}}{2} \frac{\Gamma\left(\frac{k+1}{2}\right)}{\Gamma\left(\frac{k}{2}+1\right)} \tag{5.43}$$

where Γ is the usual Gamma function.

Making use of (5.28) and (5.43), the ratio $\left(\frac{|Q|}{fP}\right)$ can be written as

$$\frac{|Q|}{fP} = 1 - \left(\frac{c}{a}\right)^k \left[1 - \frac{2}{Ck} c^{1/2-k} \sqrt{\frac{2W}{E^*}} \frac{\Gamma\left(\frac{k}{2}+1\right)}{\Gamma\left(\frac{k+1}{2}\right)}\right] \tag{5.44}$$

In order to compute the maximum $\left(\frac{|Q|}{fP}\right)$ we equate to 0 the derivative of $\frac{|Q|}{fP}$ with respect to c and evaluating $c_{c,k}$

$$c_{c,k} = \left[\frac{1}{kC}\sqrt{\frac{W}{2E^*}} \frac{\Gamma\left(\frac{k}{2}\right)}{\Gamma\left(\frac{k+1}{2}\right)}\right]^{\frac{2}{2k-1}} \tag{5.45}$$

From (5.45) one can easily get back the Hertzian case putting $k = 2$ and $C = 1/2R$. Using (5.45) and (5.44) one can obtain a clean result for every k

$$\frac{|Q|}{fP} = 1 - \left(\frac{c}{a}\right)^k \left[1 - 2k\left(\frac{c_{c,k}}{a}\frac{a}{c}\right)^{k-1/2}\right] \tag{5.46}$$

Putting $c/a = 1$, the minimum value $\left(\frac{|Q|}{fP}\right)_{\min}$ above which the interface leaves the full stick condition is

$$\left(\frac{|Q|}{fP}\right)_{\min} = 2k\left(\frac{c_{c,k}}{a}\right)^{k-1/2} \tag{5.47}$$

while the maximum value $\left(\frac{|Q|}{fP}\right)_{\max}$ is obtained for $c = c_{c,k}$ after some simple algebra

$$\left(\frac{|Q|}{fP}\right)_{\max} = 1 - (1-2k)\left(\frac{c_{c,k}}{a}\right)^k = 1 + \left(\frac{c_{c,k}}{a}\right)^{1/2}\left(1 - \frac{1}{2k}\right)\left(\frac{|Q|}{fP}\right)_{\min} \tag{5.48}$$

In Fig. 5.5 we plot (5.44) for a profile with $k = 1, 2, 4, 6$ for $c_c/a = 0.4$, showing the behavior is non monotonic with the power k. Results specific for $\left(\frac{|Q|}{fP}\right)_{\max}$ and $\left(\frac{|Q|}{fP}\right)_{\min}$ are shown respectively in Fig.6 (a-b) as a function of c_c/a for $k = [1 - 2 - 3 - 4 - 5]$. It is seen that while $\left(\frac{|Q|}{fP}\right)_{\max}$ is relatively insensitive to k at low c_c/a, the minimum $\left(\frac{|Q|}{fP}\right)_{\min}$ is very sensitive in this range. Further, a significant increase of both $\left(\frac{|Q|}{fP}\right)_{\max}$ and $\left(\frac{|Q|}{fP}\right)_{\min}$ does occur only for large c_c/a, and in this region, the actual start of microslip and inception of full slip strongly depend on geometry.

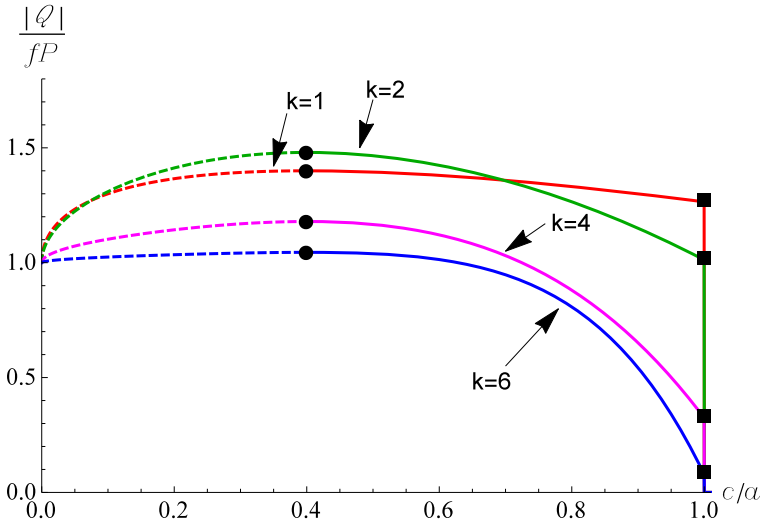

Figure 5.5. Q/fP plotted against the dimensionless width of the stick zone c/a, for $c_c/a = 0.4$, and for power law punches with $k = [1 - 2 - 4 - 6]$. For each curve the minimum $|Q|/fP$ at which partial slip commences is indicated with a black square, while the maximum value of the stable branch is indicated with a black circle.

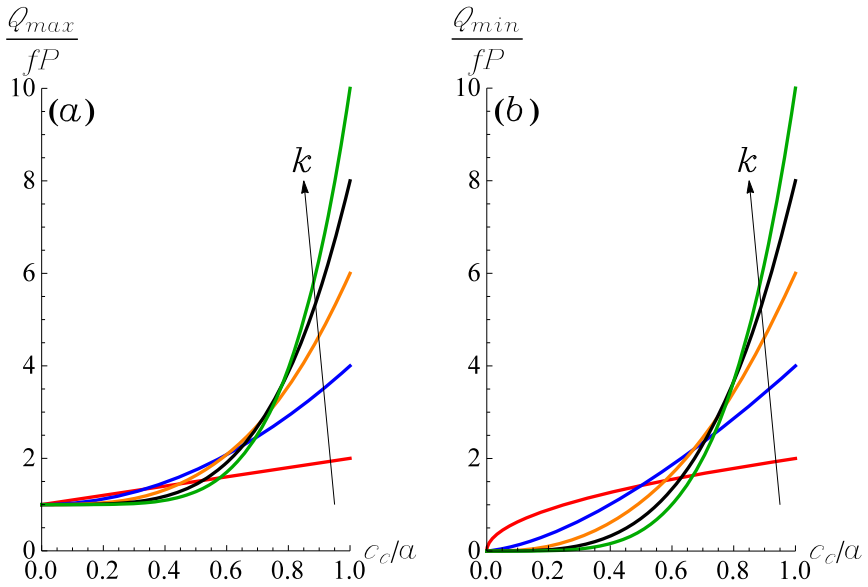

Figure 5.6. $\left(\frac{|Q|}{fP}\right)_{\max}$ and $\left(\frac{|Q|}{fP}\right)_{\min}$, respectively (a) and (b), plotted against c_c/a for $k = [1 - 2 - 3 - 4 - 5]$.

Shear tractions

From [10] the pressure distribution for a power law profile is

$$p\left(s,a\right) = -\frac{E^{*}Ck}{2}a^{k-1}r(s) \tag{5.49}$$

where

$$r(s) = \frac{1}{\sqrt{\pi}}\left[\frac{\Gamma\left(\frac{k-1}{2}\right)}{\Gamma\left(\frac{k}{2}\right)}{}_2F_1\left(1, 1-\frac{k}{2}; \frac{3-k}{2}; s^2\right)\sqrt{1-s^2} + \sqrt{\pi}\left|s\right|^{k-1}\tan\left(k\frac{\pi}{2}\right)\right] \tag{5.50}$$

and $|s| = |x/a| < 1$. Further, the function ${}_2F_1\left(1, 1-\frac{k}{2}; \frac{3-k}{2}; z\right)$ is the Gauss hypergeometric function of argument z, and the two terms in the function r should be taken with care for odd integer k as they both diverge. The shear traction then will be ($Q < 0$) within the stick area ($x \in S_{stick}$)

$$q\left(s,\bar{s}\right) = fp\left(s,a\right) - f\left[p\left(\bar{s},c\right) - \frac{\sqrt{\frac{2E^{*}W}{\pi c}}}{\sqrt{\left(1-\bar{s}^2\right)}}\right] \tag{5.51}$$

where $\bar{s} = x/c$. To make (5.51) dimensionless we divide by $p_{0,k} = \frac{E^{*}Ck}{2}a^{k-1}$, obtaining

$$\frac{q\left(s,\bar{s}\right)}{-fp_{0,k}} = r\left(s\right) - \left(\frac{c}{a}\right)^{k-1}r\left(\bar{s}\right) + \frac{4}{\sqrt{\pi}}\frac{\left(\frac{c_{c,k}}{c}\right)^{1/2}\left(\frac{c_{c,k}}{a}\right)^{k-1}}{\sqrt{\left(1-\bar{s}^2\right)}}\frac{\Gamma\left(\frac{k+1}{2}\right)}{\Gamma\left(\frac{k}{2}\right)} \tag{5.52}$$

In Fig. 5.7 (a) we plot the pressure distribution made dimensionless with $p_{0,k}$, while in Fig. 5.7 (b) we plot the shear traction made dimensionless with the mean vale q_{mean} for $c/a = 0.8$ and $c_c/a = 0.6$. It is seen that increasing k the shear tractions increase at the edge and the singularity reduces it strength at the stick-slip boundary.

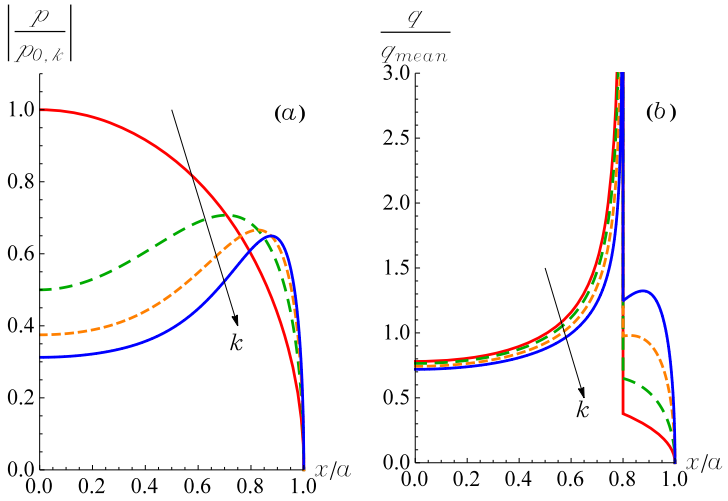

Figure 5.7. (a) Dimensionless pressure distribution $|p(x)/p_{0,k}|$ and (b) dimensionless shear tractions $q(x)/q_{mean}$ plotted against x/a for $k = [2 - 4 - 6 - 8]$, $c/a = 0.8$ and $c_c/a = 0.6$.

5.3.3 Sinusoidal wave profile

In many engineering applications periodic contact is an important model, either per se or as a basis for understanding more complicated cases which require an more than the fundamental harmonic. Let assume that the profile in contact with a half-plane has the form

$$f(x) = \Delta \cos\left(\frac{2\pi x}{\lambda}\right) \tag{5.53}$$

From the Westergaard's adhesion-less solution [68], the pressure acting over the regions $|x - n\lambda| < a$ is given by

$$p(x) = \frac{-2\overline{p}}{\sin^2(\pi a/\lambda)}\left[\sin^2(\pi a/\lambda) - \sin^2(\pi x/\lambda)\right]^{1/2} \tag{5.54}$$

while $p(x) = 0$ outside these regions, and

$$\overline{p} = -\frac{\pi E^* \Delta}{\lambda}\sin^2(\pi a/\lambda) \tag{5.55}$$

is the mean pressure acting over the cosine profile.

For periodic contact, it makes sense to consider the ratio between the mean applied shear and the value for full contact in dynamic conditions, $\frac{\bar{q}}{f\bar{p}}$, which turns out to be

$$\frac{\bar{q}}{f\bar{p}} = 1 - \left(\frac{\sin^2(\pi c/\lambda)}{\sin^2(\pi a/\lambda)} - \widetilde{W}\frac{\sqrt{(c/a)(a/\lambda)}}{\sin^2(\pi a/\lambda)}\right) \tag{5.56}$$

where we have defined a dimensionless fracture energy

$$\widetilde{W} = \sqrt{\frac{2W\lambda}{\pi E^* \Delta^2}} \tag{5.57}$$

For $2a/\lambda \ll 1$, we re-obtain curves for $\frac{\bar{q}}{f\bar{p}}$ as a function of c/a similar to the Hertzian case, and thus we omit them here. In Fig. 5.8, instead, we plot $\frac{\bar{q}}{f\bar{p}}$ for $2a/\lambda = 1$ (full contact state). It can be seen that differently for the punch-case that we have treated before, in this case the curves are concave at $c/a = 1$ and this leads to a jump from full stick into a partial slip condition without a continuous transition for load control (see dashed curve). Further increase of the tangential load result on the progress of partial slip on a stable branch and again a maximum results for which the curve becomes again unstable under load control. The cases plotted refer to 4 values of the dimensionless energy $\widetilde{W}$, from 0.01 to 1.

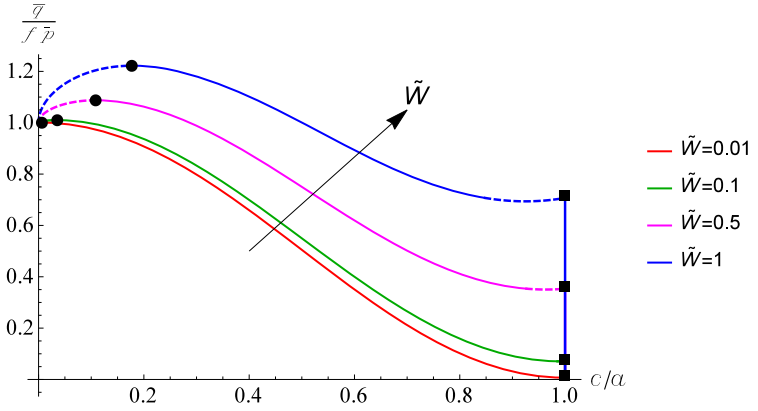

Figure 5.8. $\frac{\bar{q}}{f\bar{p}}$ plotted versus c/a for $\frac{a}{\lambda} = 0.5 = \left|\frac{a}{\lambda}\right|_{\max}$ and $\widetilde{W} = 0.01 - 0.1 - 0.5 - 1$. For each curve the minimum $|Q|/fP$ at which partial slip commences is indicated with a black square, while the maximum value of the stable branch is indicated with a black circle.

The minimum $\left(\frac{\bar{q}}{f\bar{p}}\right)_{\min}$ required to allow partial slip (not the true minimum) is that obtained for $c/a = 1$ in (5.56)

$$\left(\frac{\bar{q}}{f\bar{p}}\right)_{\min} = \widetilde{W}\frac{\sqrt{a/\lambda}}{\sin^2(\pi a/\lambda)} \tag{5.58}$$

and the maximum will be that reached for $c = c_c$. Making a derivative with respect to c will yield to a transcendental equation for the critical value c_c

$$\sqrt{\frac{c_c}{\lambda}}\sin\left(\frac{2\pi c_c}{\lambda}\right) = \frac{\widetilde{W}}{2\pi} \tag{5.59}$$

which cannot be inverted analytically, but could be computed numerically.

Shear tractions

From (5.54) and (5.3) the shear tractions will be within the stick area ($x \in S_{stick}$)

$$\frac{q(x)}{-fp_{\max}} = \left[1 - \frac{\sin^2(\pi x/\lambda)}{\sin^2(\pi a/\lambda)}\right]^{1/2} - \frac{\left[\sin^2(\pi c/\lambda) - \sin^2(\pi x/\lambda)\right]^{1/2}}{\sin(\pi a/\lambda)} + \\ + \frac{\widetilde{W}}{2\pi \sin(\pi a/\lambda)} \frac{\sqrt{\frac{c}{a}}}{\sqrt{\frac{a}{\lambda}\left[1 - \left(\frac{x}{a}\right)^2\right]}} \tag{5.60}$$

where $p_{\max} = 2\pi E^* \frac{\Delta}{\lambda} \sin(\pi a/\lambda)$. Fig. 5.9 plots $\left(\frac{\bar{q}}{f\bar{p}}\right)_{\max}$ and $\left(\frac{\bar{q}}{f\bar{p}}\right)_{\min}$ as a function of c_c/a for $\frac{2a}{\lambda} = [1 - 0.8 - 0.6 - 0.4 - 0.2]$. It is worth noticing that for low $\frac{2a}{\lambda}$ the Hertzian solution is retrieved (refer to Fig. 5.6 (a-b)), while near the full contact the curves are qualitatively different and we plot here only the case when c_c/a is low enough for $\left(\frac{\bar{q}}{f\bar{p}}\right)_{\max} > \left(\frac{\bar{q}}{f\bar{p}}\right)_{\min}$. Above this critical value, the entire loading curve is actually unstable and we switch directly from full-stick to full-sliding without partial slip intermediate condition.

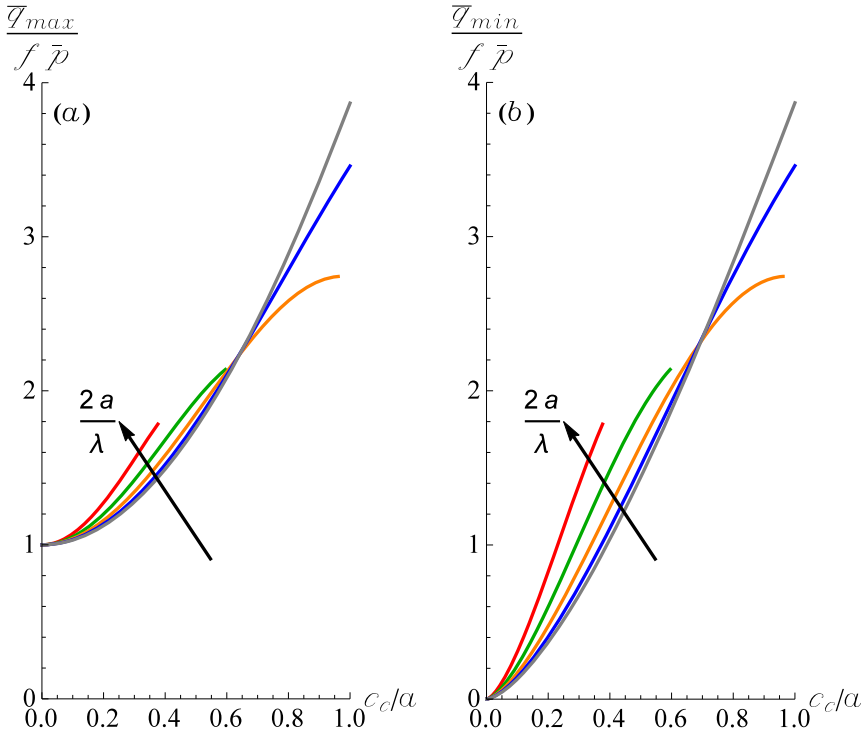

Figure 5.9. Maximum $\left(\frac{\bar{q}}{f\bar{p}}\right)_{\max}$ and minimum $\left(\frac{\bar{q}}{f\bar{p}}\right)_{\min}$ ratio of average shear to average pressure, respectively (a) and (b), plotted as a function of c_c/a for $\frac{2a}{\lambda} = [1 - 0.8 - 0.6 - 0.4 - 0.2]$.

5.3.4 Discussion

Interesting experiments were conducted on nominally Hertzian contact by Prevost *et al* [69]. They would seem to be a natural comparison element for the present theory, but the effect shown in those experiments seems opposite to what described in the present theory, namely instead of a (singular) peak of shear tractions, a distribution even smoother than the classical Cattaneo-Mindlin solution appears. We attribute this discrepancy to the fact that Prevost *et al* [69] consider friction between a rough elastomer and a smooth glass surface. Friction in rubber is certainly very different from friction between any other materials. For instance, in rubber (at low start velocity), the static friction coefficient is generally considered to be equal to the kinetic friction coefficient [70]. Prevost *et al* [69] attribute the discrepancy with respect to Cattaneo-Mindlin solution to an elastoplastic-like friction constitutive equation instead of the rigid-plastic behavior of Coulomb's law. More investigation is needed to understand why this effect doesn't seem to appear in Fineberg's group experiments. The most important result here is that geometrical effects can play a role due to the occurrence of the instability point which may explain why very small geometrical differences in the geometry may alter the apparent friction coefficient.

5.4 Conclusions

The Cattaneo partial slip contact problem has been solved with a Griffith condition for the inception of slip, and as an example we have shown the case of a single contact area with punches of power-law profile, or that of a periodic sinusoidal profile[4]. The inception to slip condition is shown to correspond under load control to an instability at a maximum tangential load, which is mathematically related to the corresponding instability of pull-off for the adhesive contact JKR solution. The dimensionless tangential force $\left(\frac{|Q|}{fP}\right)$ (normalized by the normal load and the dynamic friction coefficient) has a non-zero minimum $\left(\frac{|Q|}{fP}\right)_{\min}$ in order to start any amount of slip, and a maximum value $\left(\frac{|Q|}{fP}\right)_{\max}$ above which a load-control experiment becomes unstable and full sliding occurs. Hence, the apparent friction coefficient at inception of slip, depends on geometrical effects. In particular, for a power law profile, it is relatively insensitive to the power of the power-law polynomial k at low c_c/a (i.e. for a low fracture energy), while the minimum $\left(\frac{|Q|}{fP}\right)_{\min}$ (which gives the point of beginning of partial slip from full stick) is very sensitive in this range. A significant increase of both $\left(\frac{|Q|}{fP}\right)_{\max}$ and $\left(\frac{|Q|}{fP}\right)_{\min}$ does occur for large friction fracture energy or c_c/a, and in this region, the actual start of microslip and inception of full slip strongly depend on geometry.

[4] The case of a flat square-ended punch, tangentially loaded above the interface line is reported in Appendix A.